Melt Inclusions in Zircon

J. B. Thomas[1], R. J. Bodnar[1], N. Shimizu[2] and C. A. Chesner[3]

[1]*Department of Geological Sciences, Virginia Tech, Blacksburg, Virginia 24061*

E-mail: bubbles@vt.edu

[2]*Department of Geology and Geophysics, Woods Hole Oceanographic Institution, Woods Hole, Massachusetts 02543*

[3]*Department of Geology and Geography, Eastern Illinois University, Charleston, Illinois 61920*

INTRODUCTION

Silicate melt inclusions (MI) are small samples of melt that are trapped during crystal growth at magmatic pressures and temperatures. The MI represent a sample of the melt that was isolated from the bulk melt during host crystallization. Thus, MI preserve the composition of the melt that was present during crystal growth and record the P-T growth conditions. As such, MI provide a valuable tool for constraining the magmatic history of igneous systems. Melt inclusions may be composed of a single-phase glass or they may contain multiple phases (vapor bubbles ± crystals) that nucleated from the melt within the inclusion during cooling, or were produced by devitrification of the glass following trapping. Heating and homogenization techniques applied to multiphase MI produce a glass suitable for microanalysis, and may also provide information regarding the temperature of MI and crystal formation (Roedder 1984).

Many workers have used MI in major rock-forming minerals to constrain igneous processes, such as crystal fractionation and magma degassing (e.g., Anderson et al. 1989, Hervig and Dunbar 1992, Sobolev and Shimizu 1993, Sobolev and Danyushevsky 1994, Lu 1991), but there have been far fewer studies of MI in accessory minerals (e.g., Chupin et al. 1998, Spandler et al. 2000, Sokolov 2002, Thomas et al. 2002). Melt inclusions in zircons of igneous origin are common, and have been identified in a wide range of igneous rock types, including quartz diorite and rhyolite, and in detrital zircon grains from heavy mineral sands (Fig. 1).

The same properties that make zircon an excellent geochronometer also make zircon an ideal host for MI. Zircon is stable in most geologic environments (Watson 1996) and trace element diffusivities through the zircon crystal structure (Cherniak et al. 1997, Cherniak and Watson, this volume) are sufficiently slow to prevent exchange of components between the MI and the surrounding zircon host and/or melt, so long as the zircon crystal remains crystalline. Zircon has been of interest to petrologists for many years because it is one of the minerals that controls the rare earth element (REE) budget of crustal magmas (Nagasawa 1970, Bea 1996, O'Hara et al. 2001). The compositions of melts from which accessory minerals crystallize generally have not been well constrained, especially in plutonic rocks. As such, inverse modeling using zircon mineral chemistry and partition coefficients has been employed to back-calculate melt compositions (Hinton and Upton 1991, Guo et al. 1996, Hoskin et al. 2000, Wilde et al. 2001). Some workers have used the bulk rock as an approximation of the melt composition (e.g., Hoskin et al. 2000); however, it is difficult to unequivocally establish that a bulk rock composition represents the melt composition at any given time, especially in coarse-grained plutonic rocks. Other workers have used zircon morphology as an indicator of melt composition, magma temperature and crystallization rates (Poldervaart 1955, 1956; Pupin and Turco 1972, Vavra 1990). However, zircon morphology commonly varies considerably within any given rock, and the various chemical and physical parameters that may affect zircon morphology are poorly understood.

Melt inclusions provide an unambiguous method to directly determine compositions of melts from which zircon crystallized, provided that the MI have not leaked or re-equilibrated following

1529-6466/03/0053-0003$05.00

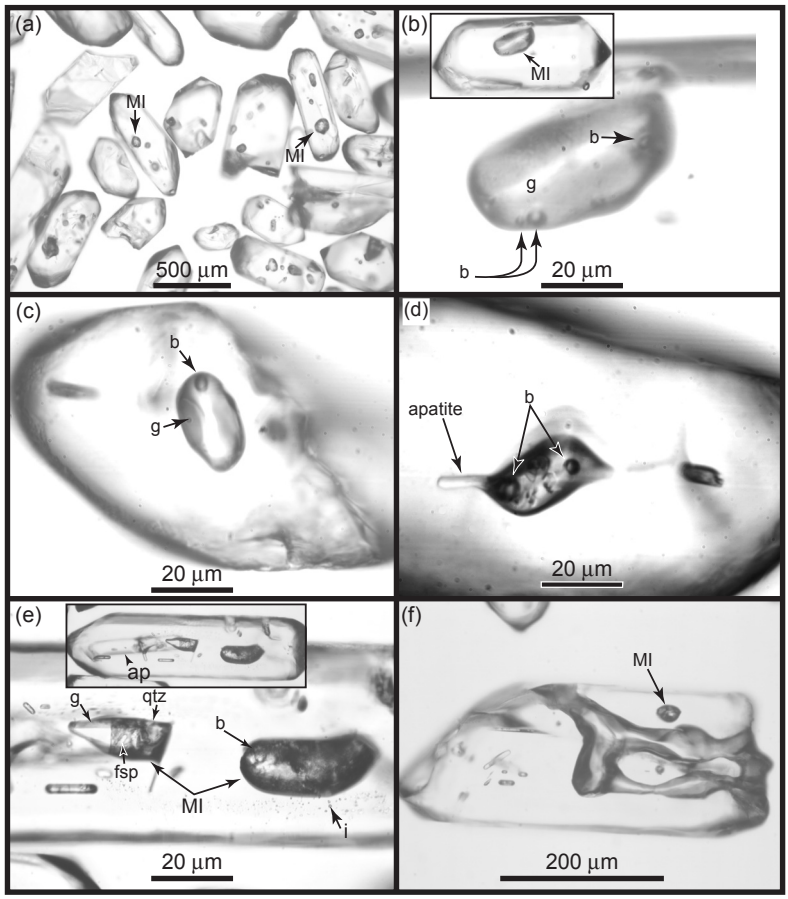

Figure 1. Transmitted light photographs of crystalline and glass melt inclusions (MI) in zircons. The zircons commonly contain solid inclusions of apatite (labeled "ap"), feldspar (labeled "fsp") and less commonly, oxide minerals. The zircons in the photographs are from: the 56 Ma quartz dioritic Quottoon Igneous Complex in British Columbia, Canada (shown in a, e and f), a rhyolitic member of the 74 ka youngest Toba Tuff of Sumatra, Indonesia (shown in b), and a heavy mineral sand deposit from north Stradbroke Island, Queensland, Australia (shown in c and d). (a) Crystalline melt inclusions in zircons extracted from the Quottoon quartz diorite. Most zircons contain dark-colored, ovoid inclusions that are crystalline melt inclusions. (b) The inset shows a low magnification photograph of a zircon from the Toba rhyolite containing an ovoid-shaped glass inclusion that is shown below the inset at higher magnification. The melt inclusion is comprised of crystal-free glass (labeled "g") and three bubbles (labeled "b"). (c) A glass melt inclusion is preserved in a rounded and broken fragment of a detrital zircon. The melt inclusion is comprised of glass and a bubble. (d) A partially crystalline melt inclusion hosted by a detrital zircon contains a crystal of apatite that was trapped along with the inclusion-forming melt. The partially crystalline melt inclusion also contains two bubbles, several transparent daughter crystals and feathery masses of dark-colored daughter crystals. (e) The inset shows a zircon from the Quottoon quartz diorite that contains a solid inclusion of apatite (labeled "ap") and two large crystalline melt inclusions that are shown below the inset at higher magnification. The large melt inclusion on the left contains a large transparent phase (glass? or quartz?), many transparent lath-shaped daughter crystals (feldspar?), a large anhedral daughter crystal (quartz? labeled "qtz"), and interstitial dark-colored daughter crystals. The large melt inclusion on the right contains a bubble that is partially obscured by daughter crystals. A decrepitation halo of small inclusions (labeled "i") occurs around the large melt inclusion on the right. (f) Zircon from the Quottoon quartz diorite containing a crystalline melt inclusion and an elongated tube-shaped inclusion that parallels the c-axis of the zircon host. The tube-shaped inclusions are commonly composed mostly of glass, however, some tube-shaped inclusions were found to be empty after the tubes were exposed at the surface.

entrapment (e.g., Qin et al. 1992, Gaetani and Watson 2000, Danyushevsky et al. 2002). As such, coupled petrographic examination (before, during and after heating) and geochemical analyses of MI and host zircons can reveal information about crystal/melt processes in igneous systems that are difficult (or impossible) to assess through conventional methods. In the first section of this chapter we summarize some of the previous studies of MI in zircon. The second section describes some general methods for preparing MI in zircons for geochemical analyses. In section three we describe the use of trace element analyses of MI and the immediately adjacent zircon to determine zircon/melt partition coefficients. Next, we discuss the significance of boundary layer development adjacent to growing crystals and compare the trace element compositions of MI in zircon with those from MI in minerals that have significantly different trace element mineral/melt partitioning behavior. The chapter concludes with some remarks regarding potential avenues for future research using MI in zircon.

PREVIOUS INVESTIGATIONS

There have been surprisingly few reports of MI in zircon. Li (1994), Chesner (1998), Chupin et al. (1998), Hoskin and Black (2000) and Frezzotti (2001) describe MI in zircon. Only two of these studies (Li 1994, Chupin et al. 1998) conducted microthermometric and/or geochemical analyses of the MI. Li (1994) focused primarily on the phase changes observed during heating of crystalline MI in zircons from southwestern and northwestern China to obtain homogenization temperatures. The crystalline melt inclusions were step-heated using one-atmosphere furnaces and heating stages. Li (1994) documented the sequence of phase changes during heating and reported homogenization temperatures ranging from 950-1100°C. Several electron microprobe analyses of MI in zircons were also reported. However, the ZrO_2 contents of these MI were very high (0.94-5.02 wt % Zr), suggesting that the analytical volume included not only melt but also zircon. Perhaps most importantly, the Li (1994) investigation demonstrated that MI occur in zircons from many different igneous environments spanning the wide compositional range from diorite to alkali syenite.

Chupin et al. (1998) performed detailed geochemical analyses of MI in zircon crystals from an Archean age greenschist facies quartzite (Witwatersrand Supergroup), a granulite facies quartzite (Beit Bridge Group) and from a granulite facies S-type granitic orthogneiss in South Africa. Zircon crystals from the Beit Bridge quartzites contained igneous cores with abundant MI, but zircon overgrowths were free of MI. These petrographic relationships were interpreted to indicate that the overgrowths were metamorphic in origin. In addition to determining the ages of detrital zircons containing MI, Chupin et al. (1998) pioneered the use of MI as a provenance tool to constrain source terranes that supplied sediments to basins in South Africa. Other studies of detrital zircon provenance have relied only upon U-Pb ages, zircon geochemistry and/or isotopic data from zircons to infer the compositions of magmas that comprised source region terranes (e.g., Wilde et al. 2001).

The MI investigated by Chupin et al. (1998) were crystalline and, therefore, required heating to dissolve daughter crystals that precipitated from the melt during cooling. The daughter crystals were optically identified as quartz, feldspar and an unidentified opaque mineral. The MI were heated using a one atmosphere heating stage mounted on a microscope. During heating, vapor bubbles were recognized as daughter crystals dissolved to form a melt. The daughter crystals melted between 750°C and 900°C. The vapor bubbles never homogenized into the melt, even when heated to 1250°C and held at that temperature for ten hours. After daughter crystals were melted, the MI were quenched to a glass containing a vapor bubble(s). Chupin et al. (1998) reported that some MI decrepitated during heating experiments, most likely due to elevated internal pressures generated in the MI during heating.

After heating and homogenization experiments, the MI were analyzed for major elements and Cl by electron microprobe. Melt inclusions in zircons from the Witswatersrand Supergroup quartzite were chemically classified as granite, trondhjemite and tonalite (Barker 1979). Melt inclusions

from the Beit Bridge Group quartzite were classified as granite and trondhjemite. Melt inclusions from the S-type orthogneiss had granitic and granodioritic compositions. Analyses of incompletely homogenized MI yielded exceptionally high concentrations of either SiO_2 (>87 wt %) or Al_2O_3 (22 wt %) or TiO_2 (2 wt %) or FeO (>3.8 wt %). Chupin et al. (1998) suggested that the unmelted crystals were trapped along with silicate melt during MI formation, because the crystals did not melt when heated to temperatures as high as 1250°C.

Based on MI compositions from detrital zircons, Chupin et al. (1998) were able to suggest several different source terranes for the sediments. The zircons in both quartzites formed in magmas of tonalitic-trondhjemitic to granitic composition that were emplaced into the sediment source regions at ~3.26 Ga. Zircons from both quartzites also had similarly rounded and pitted shapes and the crystals were interpreted as having traveled similar distances from source regions. Based on the similarity of external morphologies of the detrital zircons containing MI with tonalitic-trondhjemitic compositions with those having granitic compositions, Chupin et al. (1998) further suggested that the two sources were proximal to one another. The MI in these detrital zircons document the earliest granitoid magmatism in South Africa. The Chupin et al. (1998) study illustrates that MI compositions from detrital zircons provide important compositional information (in addition to zircon ages, geochemical/isotopic composition) that may be useful to fingerprint sediment sources.

METHODOLOGY

Melt inclusions in zircons are common but many are not suitable for geochemical analysis. Most often, the MI are rejected because they show obvious cracks intersecting the inclusion walls. In many cases only a very small proportion (~10%) of all the zircons in the rock are suitable for microthermometric and geochemical analysis. Because a given thin section may only contain a few tens (or fewer) of zircon crystals, petrographic observation of thin sections is not the most efficient means of identifying and selecting zircons for MI studies. Mineral separates are usually more suitable than thin sections for selection of zircon crystals for study. Conventional rock crushing, heavy liquid and magnetic separation are used to concentrate zircons into a mineral separate. Immersion of individual zircon crystals in refractive index oil makes it easier to observe internal features in crystals, especially if crystals have a rough surface and/or if matrix glass is attached to the crystal surfaces. Zircons containing suitable inclusions are handpicked from mineral separates under a binocular microscope using an Irwin loop. Crystalline MI are typically dark colored and polymineralic, sometimes containing a visible vapor phase. The vapor phase can be difficult to identify within crystalline MI because it commonly occurs as distorted bubbles and/or as films on daughter crystals.

Crystalline MI may be distinguished from solid mineral inclusions during careful petrographic observation using strongly collimated light, owing to the fine-grained texture of the polymineralic aggregates that formed during slow cooling. In contrast, glass inclusions are commonly clear to light brown in color and may contain one (or more) discernible vapor bubbles.

The methods used to prepare both crystalline and glass MI contained in zircons for analysis are discussed below. Melt inclusions and zircons used to illustrate these techniques are from a 56 Ma quartz diorite from the Quottoon Igneous Complex (British Columbia, Canada) and from a 74 ka rhyolite unit of the youngest Toba Tuff (Sumatra, Indonesia). Field relations, sample locations, bulk rock chemistry and petrogenesis are described in detail in Thomas and Sinha (1999; sample 2093) for the quartz diorite and in Chesner (1998) for the rhyolite. Zircons from both localities are typically clear and euhedral, and contain MI as well as solid inclusions of apatite, feldspar, and less commonly, oxide minerals. The MI from the quartz diorite were crystalline and, therefore, required heating to produce a homogeneous glass suitable for microanalysis. Techniques described for MI in the Quottoon MI would be applicable to any inclusions that crystallized or devitrified during cooling, whereas, the techniques described for the Toba MI would be applicable to glassy MI.

Petrography of melt inclusions hosted in zircon

Melt inclusions discussed in this chapter may be subdivided into two general types, glassy inclusions (Fig. 1b,c) and crystalline inclusions (Figs. 1a,d-f; see Figs. 2 and 3 below). Glass and crystalline MI are end-member types reflecting differences in the cooling rate, size and composition (including volatile content) of the trapped melt (Roedder 1979). A continuous spectrum of MI textures between the end-member types occurs depending on the geologic setting in which the zircon formed. Melt inclusions in zircon crystals from volcanic rocks are usually glassy (± vapor bubbles) due to rapid cooling of the entrapped melt after eruption (Fig. 1b). Glass MI have also been observed in detrital zircons (Fig. 1c) indicating that glass inclusions can be preserved in zircons that have undergone weathering, erosion and transport. In contrast, MI in zircons from plutonic rocks are normally crystallized to polymineralic aggregates (Figs. 1d,e). In this chapter glassy MI will be referred to as glass inclusions to distinguish them from crystalline MI. Glass MI that are the result of laboratory heating are referred to as homogenized MI.

In rapidly cooled rocks, such as plinian pumices, the entrapped melt may be quenched to a single-phase glass if cooling is sufficiently rapid, or one (or more) vapor bubbles may form with slower cooling (Fig. 1b). Some small amount of the host mineral may precipitate onto the inclusion walls during slow cooling. The amount of zircon that crystallizes onto the MI walls is generally small, compared to MI in host minerals such as quartz or feldspar. The amount of zircon that can crystallize from the melt within the inclusion is limited by the Zr content of the melt. For most felsic melts, this amount of zircon is very small because Zr concentrations are generally less than about 300 ppm (e.g., Taylor and McLennan 1981). Owing to the large amount of quartz that typically precipitates on the walls of quartz hosted MI, the size of the inclusion after heating is usually noticeably larger compared to before heating. Zircon hosted MI, however, show no discernible difference in size before and after heating.

In plutonic rocks (and in some volcanic rocks) the host phase and entrapped melt cool slowly allowing vapor bubbles and daughter crystals to nucleate and grow from the melt (Figs. 1d,e). However, some small MI remain glassy while larger MI in the same zircon crystal have crystallized to fine-grained aggregates. Crystalline MI may be composed of some mixture of glass and daughter crystals or may be entirely fine-grained aggregates of daughter crystals. Daughter crystals range from lath-shaped to anhedral feathery masses of both transparent and dark-colored minerals. The refraction of light by daughter crystal aggregates causes MI to appear dark. Petrographic observation and electron microprobe analyses of polished crystalline MI indicate that the daughter crystals in the zircon hosted MI from the Quottoon quartz diorite are mostly quartz and feldspar (Figs. 1d,e). Apatite occasionally (and feldspar rarely) occurs as a solid phase trapped with the melt that formed the MI (Fig. 1d) and as solid mineral inclusions in zircon crystals (Fig. 1e). In crystalline MI it may be difficult to distinguish between daughter crystals and trapped crystals. Trapped crystals may sometimes be identified if they extend far beyond the MI wall into the zircon host, are exceptionally large, or do not melt at temperatures similar to the homogenization temperatures recorded for other MI in the same group (Roedder 1984, Chupin et al. 1998).

Morphologies of MI in zircon range from ovoid (Figs. 1a-d) to irregularly-shaped (Fig. 2) to negative-crystal-shaped (Fig. 3a). Melt inclusions range from <1 μm to several tens or hundreds of microns in maximum dimension. The maximum dimension is limited only by the size of the host crystal. Zircons in most rocks are typically <1 mm long and, therefore, most MI in zircon are <100 μm in their longest dimension. Halos of small inclusions occur around some crystalline MI, suggesting that the MI decrepitated and expelled some of its contents into the surrounding zircon (Fig. 1e). Decrepitation halos have not been observed around glass MI in zircons, suggesting that the halos most likely form by over-pressurization of the inclusion due to volatile exsolution during crystallization of the melt within the inclusion (Roedder 1984, Student and Bodnar 1996).

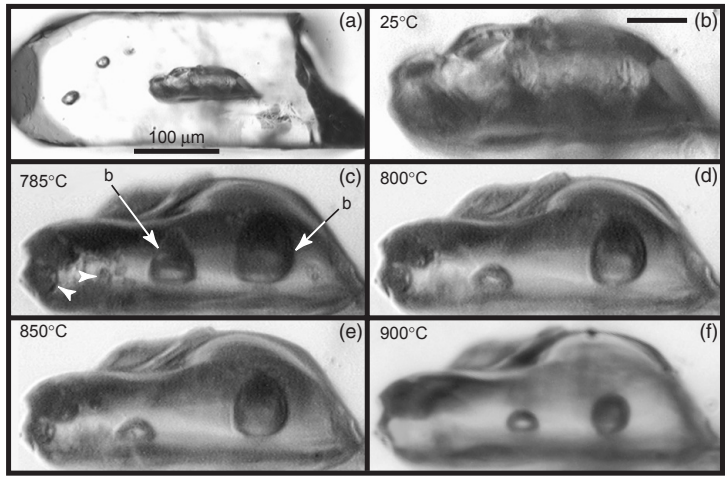

Figure 2. Transmitted light photographs of a heating sequence (~12 hours for each heating step). Zircon is from the Quottoon quartz diorite. (a) A large crystalline melt inclusion occurs near the center of the zircon and two smaller inclusions occur near the unbroken crystal termination. (b) A higher magnification photograph, taken before heating, of the large crystalline melt inclusion located near the center of the crystal. No distinct outlines of daughter crystals or bubbles are visible in the melt inclusion due to its fine-grained texture. The bar in the upper right of the photograph is 25 µm long. (c) After the first heating step at 785°C, two distinct vapor bubbles formed and several small daughter crystals (feldspar? and/or quartz?, denoted by white arrowheads) surrounded by glass were visible in the left side of the melt inclusion. (d-e) Daughter crystals and bubbles continually decreased in size during each successive heating step. (f) At 900°C the daughter crystals completely dissolved into the melt and quenching formed a glass containing two vapor bubbles. Note the increased clarity of the inclusion as the daughter crystals dissolved into the melt.

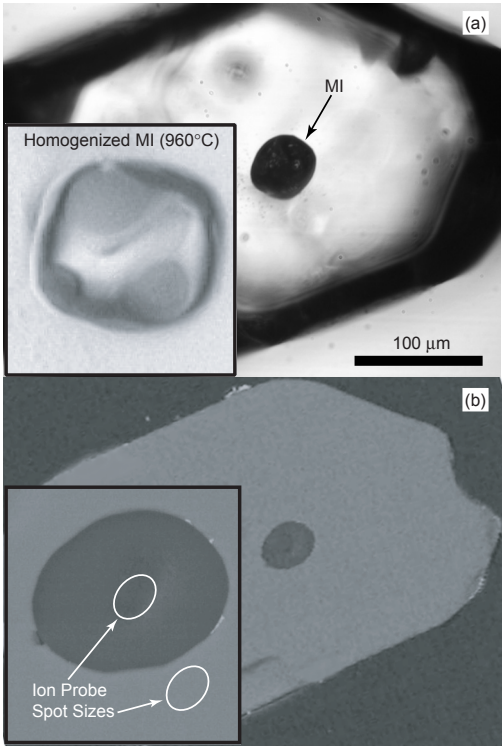

Figure 3. Melt inclusion in a zircon crystal from the Quottoon quartz diorite. (a) Transmitted light photograph of a zircon containing a crystalline melt inclusion. The inset shows an enlargement of the same inclusion after homogenization at 960°C. (b) A back-scattered electron image of the same zircon containing the homogenized melt inclusion exposed at the surface by grinding-polishing. The inset shows an enlargement of the inclusion along with representative ion probe spot sizes. [Used by permission of Elsevier Science, from Thomas et al. (2002) *Geochimica et Cosmochimica Acta*, Vol. 66, Fig. 1, p. 2889]

Heating and homogenization of crystalline melt inclusions in zircon

The applications of crystalline and glassy inclusions in igneous petrology are similar; however, a major difference is related to sample preparation for microanalysis. Glass MI do not require heating to produce a homogeneous glass for analysis, therefore, preparation simply requires exposure of the inclusion on the surface for microbeam analysis. In contrast, crystalline MI are heterogeneous aggregates of daughter crystals. Therefore, spot analyses (e.g., electron or ion microprobe) of crystalline MI would yield a mixed composition of the phases within the analytical volume of the microbeam, and not the composition of the melt originally trapped. Laboratory heating of crystalline MI is necessary to produce a homogeneous glass for analysis. Inclusions open to the surface and/or intersected by cracks should not be selected for homogenization experiments because they may not have remained closed systems after entrapment in the host crystal. Alternatively, crystalline MI may be analyzed by laser ablation inductively coupled plasma mass spectrometry (LA-ICP-MS) without the need to homogenize the inclusion. In general, a crystalline MI is positioned beneath a laser beam so that the hole drilled during ablation passes through any host crystal surrounding the inclusion and includes the entire volume of the MI into the analytical volume (Halter et al. 2002). The proportions of MI and host phase included in the analytical volume are calculated based on ratios of certain elements in the bulk rock (Halter et al. 2002).

Crystalline MI in many minerals (e.g., quartz, feldspar, pyroxene, olivine, etc.) are routinely homogenized using microscope heating stages and one-atmosphere furnaces (e.g., Sobolev and Kostyuk 1975, Roedder 1984, Kamenetsky et al. 1997, Nielsen et al. 1997). It is preferable to homogenize crystalline MI using a heating stage mounted on a microscope so that phase changes can be observed during heating. Alternatively, crystalline MI may be step-heated in a furnace and phase changes can be observed after each heating step. However, it has been our experience that heating crystalline MI at one atmosphere generates high internal pressure that commonly causes decrepitation. Decrepitation of MI and loss of volatiles results in incomplete melting of the daughter crystals that precipitated from the melt. Other workers have experienced similar problems (Chupin et al. 1998; C. Czabo 2002, pers. comm.) when attempting to homogenize crystalline MI in zircon at one atmosphere. We have successfully homogenized crystalline MI by heating them under pressure (1200-1600 bars in argon) in TZM (titanium-zirconium-molybdenum alloy) vessels, followed by rapid quenching to produce a homogeneous glass (Figs. 2 and 3). Other workers (Thomas 1994, Schmidt et al. 1998) have shown that heating inclusions under pressure minimizes decrepitation, compared to heating at one atmosphere.

To prevent losing the small crystals during heating, zircons containing crystalline MI are folded into Pt foil and inserted into unwelded Pt capsules before loading into the TZM vessel. To determine the sequence of phase changes during heating, zircons containing crystalline MI were step-heated in approximately 20°C increments, typically starting at 750°C, and held at temperature for ~12 hours. After each increment of heating, the inclusions were quenched and examined to determine the degree of homogeneity. If an inclusion had not completely homogenized, the crystals were placed back into the TZM vessel and heated to a temperature ~15-20 degrees higher than the previous step. This process was repeated until all daughter crystals were completely melted as illustrated in Figure 2. The first signs of melting typically occurred after the 750°C heating step (Fig. 2c), evidenced by increased clarity of the inclusions and recognition of vapor bubbles. Daughter crystals and bubbles progressively decrease in size during each heating step as more melt forms (Figs. 2b-f). Following homogenization and quenching, the MI contain a crystal-free glass (± vapor bubbles). The crystalline MI in zircons from the quartz diorite homogenized between 875°C and 1000°C.

Major and trace element compositions of melt inclusions in zircon

Melt inclusion compositions have been determined using a variety of microanalytical techniques. For example, major and minor element concentrations have been determined by electron

microprobe (Morgan and London 1996), trace element and isotopic abundances have been determined by SIMS, secondary ion mass spectrometry (Shimizu and Hart 1982, Hervig et al. 1989, Sisson and Layne 1993, Webster and Duffield 1991, Shimizu et al. 1997, Shimizu 1998), LA-ICP-MS (Halter et al. 2002), and volatile contents have been determined by FTIR or Raman spectroscopy (Anderson et al. 1989, Ihinger et al. 1994, Lowenstern 1994, Thomas 2000). When developing an analytical protocol, nondestructive techniques, such as electron microprobe and Raman spectroscopy, should be employed first, followed by destructive techniques such as SIMS and LA-ICP-MS. Here we describe an analytical protocol involving electron microprobe and SIMS analyses, designed to determine major element and REE and other trace element abundances in MI. We first conduct major and minor element analyses of the MI and host zircons using an electron microprobe followed by trace element analyses using SIMS. With this analytical protocol, zircons containing glass MI were cast in epoxy and ground-polished to expose the inclusion at the surface. Thomas and Bodnar (2002) describe a method for mounting individual zircon crystals so that each zircon can be ground and polished to expose a pre-selected MI at the crystal surface.

Major and minor element compositions of the melt inclusions were determined at Virginia Tech with a Caméca® SX-50 electron microprobe equipped with four wavelength-dispersive spectrometers enabling four elements to be measured simultaneously. For glass (melt inclusion) analyses, an accelerating voltage of 15 kV was used with a beam current of 2-5 nA, and a beam diameter <5 μm. Na and K were measured in the first 30 s to minimize the effect of volatilization. For electron microprobe analyses of zircon the beam current was increased to 100 nA with a beam diameter of ~1 μm. Analytical schemes for melt inclusions and zircons used 20-40 s counting times (peak and background) for major elements; for minor and trace elements the counting times were 60-600 s. Initial standardization was performed with a combination of minerals and glasses similar in composition to the melt inclusions and the host zircons. The accuracy of major element data is better than ±2% relative, and the accuracy of minor element analyses varies from 2-10% relative.

Trace element abundances were measured with a Caméca® IMS 3f ion microprobe at Woods Hole Oceanographic Institution using previously described procedures (e.g., Shimizu and Hart 1982, Shimizu et al. 1997, Shimizu 1998). Gold-coated polished sections were analyzed using a primary O^- beam with a primary beam current of ~1 nA. A beam diameter of ~12-15 μm was used for REE analyses. Molecular ion interferences were suppressed by offsetting the secondary-ion accelerating voltage by 60 V for REE with an energy window of ±10 V using an energy-filtering technique (Shimizu and Hart 1982). Element abundances were determined by converting secondary-ion intensity (ratioed against silicon), using empirical relationships between intensity and concentration based on analyses of rhyolite glass standards. Analytical uncertainties are mainly due to counting statistics (5-15% for the REE).

Some typical analytical results obtained from homogenized crystalline MI from the Quottoon quartz diorite and from glass MI from the Toba rhyolite are described below. Petrographic observations (Figs. 1, 2 and 3a), back-scattered electron imagery (Fig. 3b), electron microprobe major element traverses and electron microprobe/SIMS trace element traverses confirmed the chemical homogeneity of individual MI (including homogenized crystalline inclusions) and the host zircon crystals. SiO_2 contents range from 68.9 to 74.9 wt % for MI in zircons from the quartz diorite and from 74.9 to 78.8 wt % for MI in zircons from the rhyolite (Fig. 4). The major element concentrations show little correlation with SiO_2 content (Fig. 4). Other than SiO_2, no systematic differences are observed between major element concentrations of MI in zircon grains from the quartz diorite and those from the rhyolite. In both cases, melts that precipitated zircon are calc-alkaline, peraluminous and chemically classified as granite (or rhyolite; Barker 1979, Cox et al. 1979).

Chondrite-normalized (Nakamura 1974) REE abundances of MI and the immediately adjacent zircon host are shown in Figure 5. Melt inclusions display smooth U-shaped chondrite-normalized REE patterns (Figs. 5a,b) that differ significantly from the host zircons (Figs. 5c,d). La_N/Yb_N ratios (where the subscript N refers to the chondrite normalized concentration) for MI from the

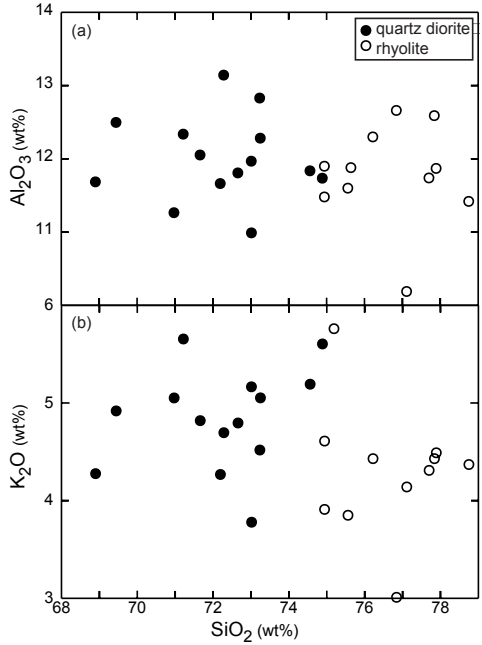

Figure 4. Major element variation diagrams for SiO_2 vs. (a) Al_2O_3 and (b) K_2O for melt inclusions in zircon from the Quottoon quartz diorite and from the Toba rhyolite.

quartz diorite range from 0.63 to 7.51 (average = 2.6) and from 0.42-8.33 (average = 2.14) for MI from the rhyolite, indicating that light REE are not strongly fractionated from heavy REE (Figs. 5a,b). The highest La_N/Yb_N ratios correspond to inclusions with the lowest Yb abundances. While the light REE are not strongly fractionated from the heavy REE in MI, light REE are somewhat fractionated from the middle REE (Figs. 5a,b) as shown by the U-shaped chondrite-normalized REE patterns. With the exception of two analyses of MI from the quartz diorite, the REE abundances of the MI and zircons from the quartz diorite and from the rhyolite are similar.

The zircon crystals analyzed are enriched in heavy REE, but depleted in the light REE, relative to the melt inclusions (Figs. 5c,d). With the exception of Ce, concentrations of REE in zircon increase smoothly from La to Yb. Zircon crystals

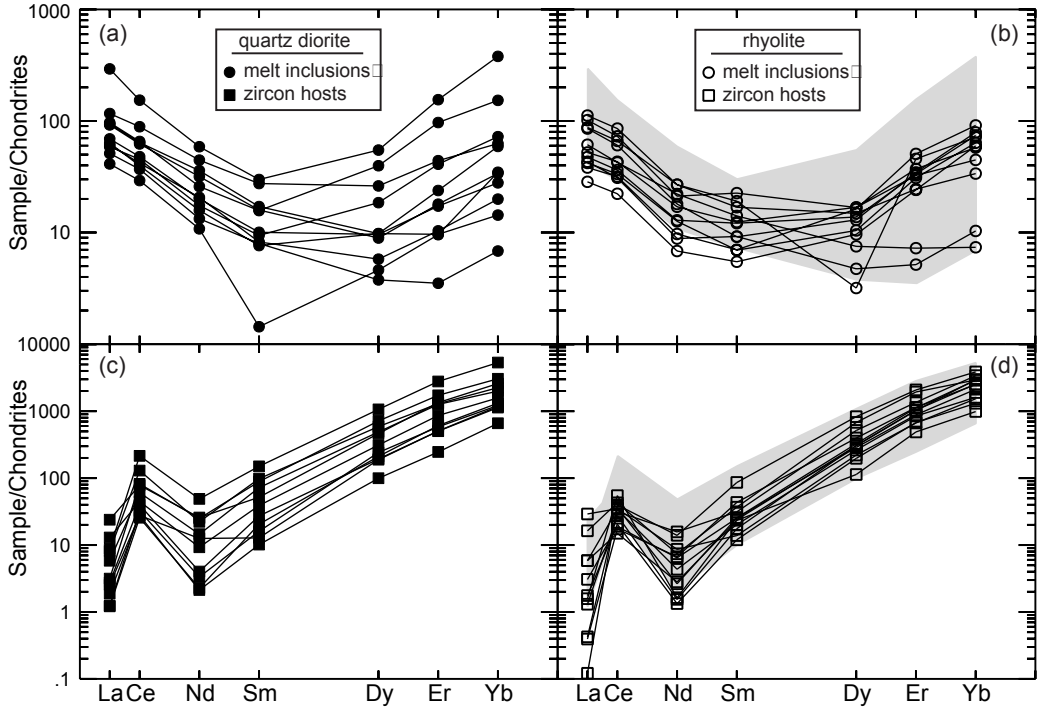

Figure 5. Chondrite-normalized rare earth element abundances of melt inclusions and zircon hosts from the Quottoon quartz diorite and the Toba rhyolite. The gray-shaded overlays in (b) and (d) outline the rare earth element patterns of the melt inclusions and zircons from the quartz diorite.

display large positive Ce anomalies ($Ce/Ce^* = Ce_N/\sqrt{[La_N \times Nd_N]}$) ranging from 3.16 to 15.8 (average = 9.4) for zircon crystals from the quartz diorite and from 2.34 to 36.4 (average = 13.76) in zircon crystals from the rhyolite. The La_N/Yb_N ratios of the zircons from the quartz diorite range from 0.00093 to 0.00927 (average = 0.00333) and the La_N/Yb_N for zircons from the rhyolite range from <0.001 to 0.019 (average = 0.004). Total REE of the zircon crystals (for the seven REE analyzed in the zircon crystals) from the quartz diorite range from 263 to 2411 ppm (average = 910 ppm) and from 388 to 1662 ppm (average = 930 ppm) for zircon crystals from the rhyolite. This range is consistent with abundances for these same REE measured in zircon crystals from other felsic igneous rocks (Hoskin et al. 2000).

DETERMINING ZIRCON/MELT TRACE ELEMENT PARTITION COEFFICIENTS USING MELT INCLUSIONS IN ZIRCON

In this section we describe the application of trace element analyses of MI and host zircon to determine zircon/melt (= zc/melt) partition coefficients ($^{zc/melt}D_M$, where the subscript M refers to the trace element of interest). The melt inclusion-mineral (MIM) technique was used to calculate partition coefficients for the REE (La, Ce, Nd, Sm, Dy, Er and Yb) and Ba, Rb, B, Sr, Ti, Y and Nb, based on analyses of natural MI contained in zircon crystals. The MIM technique combines many of the advantages of conventional techniques used previously to determine $^{zc/melt}D_M$, while at the same time minimizing or eliminating many of the drawbacks of those techniques (e.g., accidentally including small crystals in the glass separate). Most previous partitioning studies used bulk analyses of zircon and either coexisting glass or whole rock separates to represent the melt composition (Nagasawa 1970, Mahood and Hildreth 1983, Murali et al. 1983, Fujimaki 1986, Bea et al. 1994). Watson (1980) determined $^{zc/melt}D_M$ for La, Sm, Ho, and Lu using synthetic zircon crystals grown from peralkaline melts (with no additional element(s) added for charge compensation, e.g., P^{5+} to utilize the xenotime substitution).

With the MIM technique, trace element concentrations in MI and in the immediately adjacent host mineral are measured by SIMS and used to calculate *in situ* mineral/melt partition coefficients. Lu et al. (1992) and Sobolev et al. (1996) pioneered this technique to determine partition coefficients in mineral/melt systems. The technique has been extended to determine zircon/melt partition coefficients for REE and other trace elements in felsic systems (granitic and rhyolitic), using crystalline MI in zircon extracted from a quartz diorite of the Quottoon Igneous Complex in British Columbia, Canada (Thomas et al. 2002) and from a rhyolite of the Toba Tuffs in Sumatra, Indonesia (Chesner 1998). The partition coefficients obtained from analyses of homogenized MI and zircon hosts from the quartz diorite are comparable to those obtained from analyses of unheated glass MI and zircon hosts from the Toba rhyolite.

Trace element partitioning data and interpretations

Rare earth element partitioning. Zircon/melt partition coefficients for each zircon/MI pair are listed in Table 1 and shown on Figure 6a. Zircon/melt REE partition coefficients increase with increasing atomic number—the trend is similar to that determined by other workers (Nagasawa 1970, Hinton and Upton 1991, Watson 1980, Fujimaki 1986, Guo et al. 1996, and others; see also the compilation at the GERM website at: http://earthref.org/GERM/). While the concentrations of individual trace elements vary by more than one order of magnitude from one MI to the next (Fig. 5a) and from one zircon crystal to the next (Fig. 5c), the calculated partition coefficients for individual REE generally vary by less than one order of magnitude (Table 1), reflecting the fact that MI with the highest REE abundances are generally associated with zircon crystals with the highest REE abundances. For example, the La concentration in the MI from the Quottoon Igneous Complex zircon crystals varies from about 14 to 97 ppm, and the La concentration in host zircon ranges from 0.4 to 7.89 ppm. Assuming that the La concentrations in MI and zircon host vary randomly, one could expect a range in calculated $^{zc/melt}D_{La}$ of greater than two orders of magnitude (from 0.0041 to

Table 1. Zircon/melt partition coefficients (D_{REE}) calculated using REE abundances of melt inclusions and coexisting zircon crystals from the Quottoon Igneous Complex and from the Toba rhyolite. [Quottoon Igneous Complex data used by permission of Elsevier Science, from Thomas et al. (2002) *Geochimica et Cosmochimica Acta*, Vol. 66, Table 3, p. 2894]

	D_{La}	D_{Ce}	D_{Nd}	D_{Sm}	D_{Dy}	D_{Er}	D_{Yb}
	0.05	2.06	1.58	11.61	72.98	72.39	51.52
	0.04	0.83	0.2	2.7	20.09	29	40.63
	0.07	1.46	0.5	3.56	22.45	29.35	35.88
	0.22	0.99	0.53	4.14	16.79	21.09	21.9
	0.03	1.4	0.77	5.02	19.41	17.89	14.04
Quottoon	0.02	0.61	0.11	2.49	36.56	58.88	66.1
	0.06	0.93	0.56	4.58	12.37	13.07	13.04
	0.26	1.26	0.81	3.24	51.95	74.99	76.32
	0.02	0.43	0.35	0.75	19.31	52.72	82.29
	0.03	1.1	0.31	11.24	52.31	60.74	35.11
	0.05	0.75	0.16	1.27	26.42	70	96.72
Median D_M	0.05	0.99	0.5	3.56	22.45	52.72	40.63
	0.21	0.67	0.41	4.28	11.77	20.29	16.51
	0.04	0.56	0.10	0.99	14.29	20.23	17.70
	0.01	0.56	0.76	4.71	84.12	220.81	242.70
	0.43	1.35	0.76	5.25	41.83	38.21	32.13
	0.03	0.83	0.12	2.52	29.45	33.56	39.92
Toba	0.03	0.29	0.24	1.32	90.39	19.27	29.74
	0.01	0.74	0.71	2.22	68.45	187.43	460.31
	0.001	0.55	0.66	3.81	49.48	63.81	86.30
	0.001	0.42	0.10	1.52	22.04	45.75	85.86
	0.02	0.90	0.09	2.61	23.42	29.67	37.44
	0.08	0.17	0.16	0.43	14.48	27.56	36.77
Median D_M	0.03	0.62	0.25	2.37	26.44	31.61	37.10

Table 2. Zircon/melt partition coefficients (D_M) calculated for lowest (top row) and highest (bottom row) La, Sm and Yb abundances in the melt inclusions and zircon hosts. [Used by permission of Elsevier Science, from Thomas et al. (2002) *Geochimica et Cosmochimica Acta*, Vol. 66, Table 4, p. 2896]

$^{a}La_{MI}$	$^{b}La_{zircon}$	D_{La}	$^{a}Sm_{MI}$	$^{b}Sm_{zircon}$	D_{Sm}	$^{a}Yb_{MI}$	$^{b}Yb_{zircon}$	D_{Yb}
13.6	0.41	0.03	0.29	3.26	11.24	1.495	144.6	96.72
96.6	2.9	0.03	6.06	30.4	5.02	83.35	1170	14.04

(a) REE abundance in melt inclusion.
(b) REE abundance in zircon.

0.563). However, partition coefficients calculated for the two end-member melt concentrations reported above are identical at 0.03 (Table 2), and the total range in $^{zc/melt}D_{La}$ is only about one order of magnitude (from 0.02 to 0.26; Table 1). The variations in partition coefficients determined using the MIM technique are consistent with those determined in both experimental studies (Watson 1980) and from analyses of natural samples (Mahood and Hildreth 1983). Watson (1980) reports a range in $^{zc/melt}D_{Lu}$ from less than 20 to greater than 100 based on experimental data, and Mahood and Hildreth (1983) report a range in $^{zc/melt}D_{La}$ from 7.2 to 26.6 based on analyses of zircon and rhyolitic glass from the Bishop Tuff of the Long Valley caldera in California, U.S.A.

In a dynamic crystallizing igneous system, major and trace element abundances vary as crystallization proceeds. The range in REE contents of MI and zircon shown in Figures 5a-d reflects this natural variation in REE abundances in igneous systems. Based on the occurrence of zircon in early crystallizing plagioclase and also in later crystallizing biotite and quartz, zircon is believed to have formed over a significant portion of the crystallization history. As such, the REE budgets of the melt and the zircons precipitating from that melt would be expected to vary with time as the melts evolve during crystallization of zircon and other minerals. The variation of $^{zc/melt}D_M$ observed at the individual single zircon host/MI scale determined using the MIM technique is similar to the variation observed at the zircon separate/bulk rock (or glass) scale in other studies (e.g., Mahood and Hildreth 1983).

The mechanism by which REE substitute into the zircon structure is fairly well understood. The zircon structure contains two sites for cation substitution, a tetragonal Si and a larger triangular dodecahedral Zr^{4+} *site* (Speer 1982, Finch and Hanchar, this volume). Heavy REE enrichment is due to substitution into the site containing Zr^{4+} (Speer 1982). Xenotime-type substitution (whereby

a REE^{3+} ion and P^{5+}—or some other pentavalent cation—substitute for Zr^{4+} and Si^{4+}) has been reported in zircon (e.g., Speer 1982, Hinton and Upton 1991, Hoskin et al. 2000, Hanchar et al. 2001, Finch et al. 2001). However, this substitution mechanism is minimal in zircons described here, presumably because of low concentrations of P in the melts (Thomas et al. 2002), so some other element(s) must assist in charge-balancing the trivalent REEs and Y.

The compatibility of REE^{3+} in zircon is controlled mostly by REE^{3+} radii (Hinton and Upton 1991, Guo et al. 1996). As such, ${}^{zc/melt}D_{REE}$ increase from La through Yb as the ionic radii decrease from 1.16 Å to 0.985 Å, and approach the ionic radius of Zr^{4+} (0.84 Å; ionic radii in VIII-coordination are from Shannon 1976). Due to differences in the ionic radius of Zr^{4+} compared to radii of the REE^{3+}, substitution of REE^{3+} for Zr^{4+} in the zircon structure results in lattice strain. Blundy and Wood (1994) and Wood and Blundy (1997) describe a method based on a lattice strain model developed by Brice (1975) to predict partitioning behavior in mineral/melt systems. According to this model, partition coefficients should display a parabolic form when log ${}^{mineral/melt}D_M$ is plotted versus ionic radii for a group of isovalent cations. The maximum on the parabola defines the optimum cation size that fits into the site involved in the partitioning (Onuma et al. 1968), and it is generally close to the size of the major cation that is being replaced. For zircon, the maximum on the parabola should be at approximately 0.84 Å, which corresponds to the ionic radius of Zr^{4+} in the zircon structure (Speer 1982, Shannon 1976). However, it should be noted that several investigations have shown that the optimal size of the cation that fits into the site onto which partitioning occurs increases as the trace element charge decreases (Van Westrenen et al. 2000, Hill et al. 2000). Therefore, the maximum on the parabola may in fact be somewhat greater than 0.84 Å for the partitioning of REE^{3+} cations into the Zr^{4+} site.

The ${}^{zc/melt}D_{REE}$ values predicted from the Brice (1975) equation are compared to values calculated from MI and zircon analyses on Figure 6. The predicted ${}^{zc/melt}D_{REE}$ were obtained using 0.84 Å as the optimum cation radius (r_o) of the Zr site onto which partitioning occurs, a Young's modulus for the Zr site (E) of 2003 kbar, and the homogenization temperatures obtained from each MI (Thomas et al. 2002). The Young's modulus was derived by fitting partitioning data to Equation (10) of Wood and Blundy (1997) and then using the relationship between Young's modulus and bulk modulus described by Hazen and Finger (1979) and shown in Blundy and Wood (1994; their Fig. 3). The Brice (1975) model requires that the partition coefficient for one cation of the isovalent group be known in order to calculate partition coefficients for other elements of the isovalent group. In the model calculations shown on Figure 6, the value ${}^{zc/melt}D_{Sm}$ from each zircon/MI pair was used to represent the "known" (D_a) value for that inclusion. The predicted values shown on Figure 6b define only one limb of the parabola because the radius of the Zr site (0.84 Å) is smaller than the radius of the smallest REE (Yb) measured. The maximum on the parabola is at a radius of 0.84 Å and lies off of the diagram to the left. The partition coefficients predicted by the Brice (1975) equation lie within the range of ${}^{zc/melt}D_{REE}$ for all of the REE measured using the MIM technique, and the predicted values vary by less than one order of magnitude from the median ${}^{zc/melt}D_{REE}$ values reported in Table 1 (except for Ce, which is discussed in more detail below).

Partition coefficients predicted by the Brice equation from the MI data are compared to published values on Figure 6c. All studies, including data obtained using the MIM technique (Thomas et al. 2002), show an increase in compatibility with decreasing ionic radius. However, in contrast to most previously published results (with the exception of the data of Murali et al. 1983), the MIM data indicate that La and Nd are not partitioned into zircon in felsic melts (i.e., ${}^{zc/melt}D_M < 1$). Petrogenetic implications of this difference are considered later. Most previous studies show flat partitioning patterns for the light through middle REE (i.e., no change in the partition coefficient with ionic radius), whereas MIM results indicate continuously decreasing compatibility from Yb through La as predicted by the Brice equation. Watson (1980) shows the same general pattern as determined by the MIM technique (Fig. 5c), although the absolute values for ${}^{zc/melt}D_M$ between the two studies differ by more than one order of magnitude for La (and less for the other REE). These differences

may be related to differences in melt compositions between these two studies (i.e., peralkaline versus granitic, respectively). Note that the $^{zc/melt}D_{LREE}$ trends from previously published studies are opposite of that predicted by the Brice (1975) model. Hinton and Upton (1991) noted that many published $^{zc/melt}D_{LREE}$ are significantly higher than would be expected if REE substitution is exclusively a function of ionic radius, and that the high partition coefficients from these studies may be affected by impurities contained in zircon separates.

Differences in calculated $^{zc/melt}D_M$ described above also reflect the different experimental and analytical techniques employed in these various studies. Hinton and Upton (1991), Maas et al. (1992) and Guo et al. (1996) suggested that many of the reported $^{zc/melt}D_M$ values may have large errors associated with them owing to bulk analysis of zircons containing solid inclusions or altered zircons, and other workers have documented the significant effects of small amounts of contaminants during analysis (Michael 1988, Beattie 1994). Our calculations indicate that including less than 0.01 to 0.001% of an accessory mineral that strongly partitions the LREE (e.g., allanite or mona-

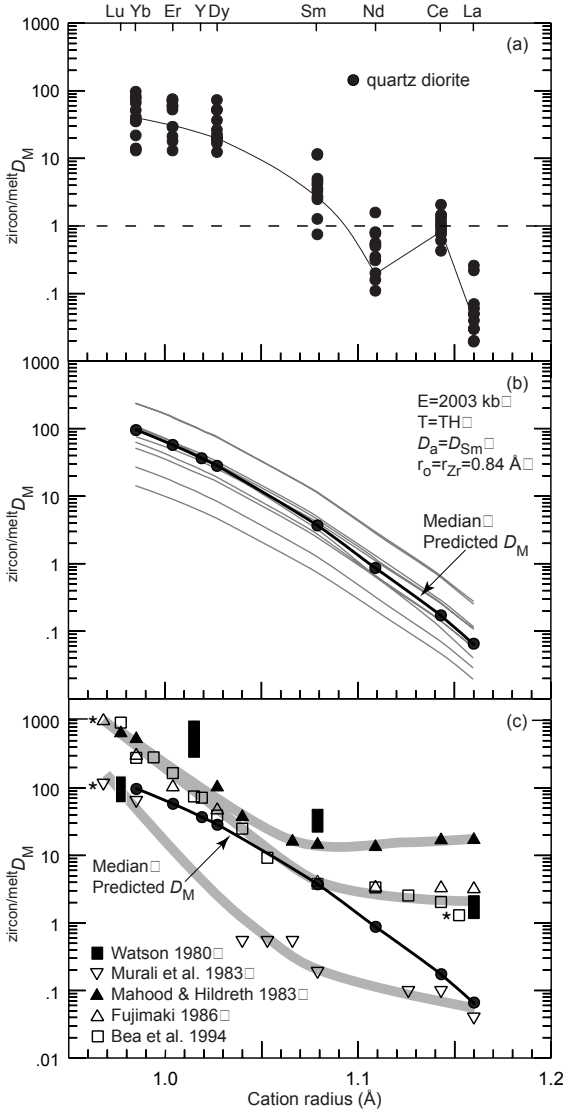

Figure 6. Zircon/melt partition coefficients ($^{zc/melt}D_{REE}$) vs. cation radii of the rare earth elements (cation radii in VIII-coordination are from Shannon 1976). The homogenized melt inclusions in zircons used to determine partition coefficients are from the Quottoon quartz diorite. (a) $^{Zc/melt}D_{REE}$ calculated from secondary ion mass spectrometric analyses of host zircon/MI pairs. The calculated values are listed in Table 1. The line connects values determined from one zircon/MI pair and shows the expected parabolic trend (see Fig. 6b) as well as the significant Ce anomaly. Similar trends are exhibited by the other ten inclusions, but are not shown because the overlap in data makes it difficult to identify lines connecting individual inclusions. The dashed line separates the elements that are compatible in the zircon crystal structure (i.e., $^{zc/melt}D_{REE}$ >1) from elements that are incompatible in the zircon crystal structure. (b) $^{Zc/melt}D_{REE+Y}$ predicted by the Brice (1975) calculated using the measured homogenization temperature for each melt inclusions (see text for details). The heavy solid line defines the median predicted partition coefficient (D_M). (c) Comparison of median predicted D_M to previously published results. The upper shaded line shows the trend for the data of Mahood and Hildreth (1983), the middle shaded line approximates the trends for the data of Fujimaki (1986) and Bea et al. (1994), and the lower shaded line shows the trend for the data of Murali et al. (1983). Five of the data points (denoted by asterisks) from previous studies have been offset to the along the cation radius axis to avoid overlapping of the symbols. [Used by permission of Elsevier Science, from Thomas et al. (2002) *Geochimica et Cosmochimica Acta*, Vol. 66, Fig. 7, p. 2895]

zite) within the bulk sample could produce the observed flat $^{zc/melt}D_{LREE}$ pattern reported by other workers (Fig. 6c). We suggest that the good agreement between model results predicted by the Brice equation and those obtained using the MIM technique, indicate that $^{zc/melt}D_{REE}$ obtained using the MIM technique may have smaller errors compared to those obtained from bulk analyses of mineral separates because "pure" zircon and/or glass separates may be impossible to obtain.

Positive Ce anomalies in zircon. Terrestrial zircon commonly shows a positive Ce anomaly (Murali et al. 1983, Hinton and Upton 1991, Ireland and Wlotzka 1992), which has been interpreted to indicate the incorporation of Ce^{4+} into zircon. Because Ce^{4+} has the same charge and a similar ionic radius (Ce^{4+} = 0.97; Zr^{4+} = 0.84 Å) as the Zr^{4+} it replaces, it is incorporated into the zircon structure much more readily than the larger Ce^{3+} (Ce^{3+} = 1.143 Å). Thus, the calculated partition coefficient for Ce (Fig. 6a) represents an apparent partition coefficient that includes both Ce^{3+} and Ce^{4+} (Hinton and Upton 1991). The strong positive Ce anomalies in zircon (e.g., Murali et al. 1983, Hinton and Upton 1991, Maas et al. 1992, Guo et al. 1996, Hoskin et al. 2000, Ireland and Wlotzka 1992) indicate that Ce occurs in melts as both Ce^{4+} and Ce^{3+}, although Ce^{3+} dominates in terrestrial melts (Schreibber et al. 1980). Ce anomalies are absent in most lunar zircons (Hinton and Myer 1991, Wopenka et al. 1996) that formed under reducing conditions.

The expected partition coefficient assuming 100% Ce^{3+} was calculated using the Brice (1975) equation described earlier. Using the same values for the input parameters as described above for the other REE^{3+} gives $^{zc/melt}D_{Ce^{3+}}$ = 0.14 (Fig. 6b). The median value for the apparent partition coefficient for Ce determined from the MIM technique is 0.99 (Table 1). The partition coefficient for Ce^{4+} in zircon was predicted using the ionic radius for Ce^{4+} (0.97 Å), a Young's modulus (E) for the site of 4226 kbar (based on the relationship between cation charge/site volume ratio (Z/d^3) and bulk modulus, after Hazen and Finger (1979) and using $^{zc/melt}D_{Zr^{4+}}$ = 1700 (based on the average Zr concentration in the MI and host zircon). Using these values, the median value predicted by the Brice (1975) equation is $^{zc/melt}D_{Ce^{4+}}$ = 102.6.

The Ce^{4+}/Ce^{3+} ratio in the MI was estimated using the calculated $^{zc/melt}D_{Ce^{4+}}$ and $^{zc/melt}D_{Ce^{3+}}$ values, the apparent $^{zc/melt}D_{Ce}$ values from Table 1, and equation 2 from Hinton and Upton (1991). The calculated Ce^{4+}/Ce^{3+} ratios range from 0.0029 to 0.0188, and (except for one value) show a systematic increase in Ce concentration in zircon with increasing Ce^{4+}/Ce^{3+} ratio in the melt, suggesting that zircons with the highest Ce content crystallized from melts with the highest Ce^{4+}/Ce^{3+} ratios. The wide range in Ce concentration in zircon is likely the result of variable Ce and evolving Ce^{4+}/Ce^{3+} ratio in the melt during crystallization. It should be noted, however, that zircons with positive Ce anomalies (reflecting an elevated concentration of Ce^{4+} in the zircon) can be produced from melts with relatively low Ce^{4+}/Ce^{3+} (Hinton and Upton 1991).

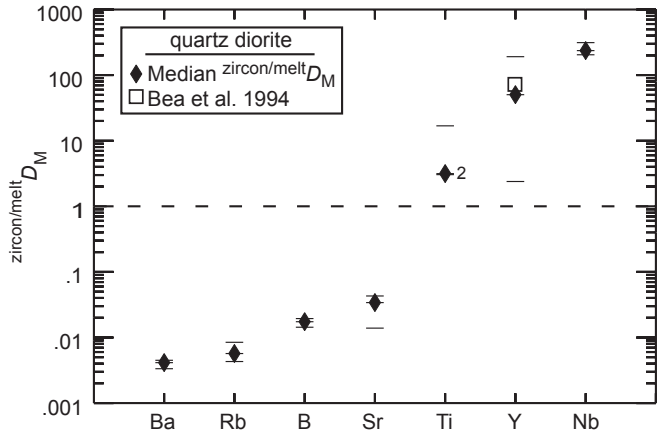

Figure 7. Trace element $^{zc/melt}D_M$ determined from zircon/melt inclusion pairs from homogenized melt inclusions in zircon from the Quottoon quartz diorite. The elements are plotted in terms of increasing compatibility in zircon. Tic marks indicate individual values, and the "2" adjacent to the tic mark for Ti indicates two data points with overlapping values. Also shown for comparison is a single value for $^{zc/melt}D_Y$ from the literature (Bea et al. 1994). The dashed line is the same as in Figure 6a. [Used by permission of Elsevier Science, from Thomas et al. (2002) *Geochimica et Cosmochimica Acta*, Vol. 66, Fig. 8, p. 2897]

Table 3. Zircon/melt partition coefficients (D_M) calculated from the trace element concentrations of three melt inclusions and their coexisting zircon hosts. [Used by permission of Elsevier Science, from Thomas et al. (2002) *Geochimica et Cosmo-chimica Acta*, Vol. 66, Table 5, p. 2897]

	D_{Ba}	D_{Rb}	D_B	D_{Sr}	D_{Ti}	D_Y	D_{Nb}
	0.003	0.008	0.019	0.034	3.30	50.2	312
	0.005	0.006	0.014	0.043	16.8	191	236
	0.004	0.004	0.017	0.014	3.15	2.39	204
Median D_M	0.004	0.006	0.017	0.034	3.30	50.2	236

Other trace elements. In addition to REE, the MIM technique may be used to determine partitioning behavior of a wide range of other trace elements. For example, zircon/melt partition coefficients for Ba, Rb, B, Sr, Ti, Y and Nb were obtained using the MIM technique (Table 3). Zircon/melt partition coefficients for these elements were calculated as described above for the REE, and are plotted on Figure 7 in terms of increasing compatibility. $^{Zc/melt}D_M$ values are listed in Table 1. As expected based on charge/size ratios, Ba, Rb, B and Sr behave incompatibly, whereas Y and Nb are highly compatible, with Ti showing moderate compatibility. These values are consistent with elevated Nb and Y concentrations often reported for zircon (cf. Hoskin et al. 2000), and with the single value for $^{zc/melt}D_Y$ from Bea et al. (1994).

Petrogenetic implications

Partition coefficients are required for quantitative modeling of petrogenetic processes and relatively small errors in partition coefficients can significantly affect model predictions. To illustrate this, we have modeled batch partial melting (Shaw 1970) and fractional crystallization (Greenland 1970) using the $^{zc/melt}D_{La}$ and $^{zc/melt}D_{Yb}$ determined using the MIM technique and compared these results to those predicted using the partition coefficients of Fujimaki (1986). We se-

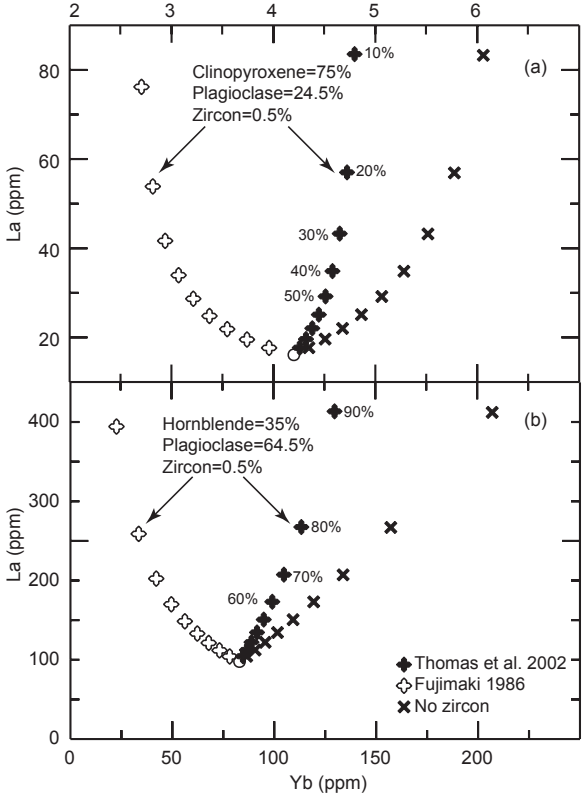

Figure 8. Petrogenetic models for (a) batch partial melting (Shaw 1970) and (b) fractional crystallization (Greenland 1970) showing the effect of variation in $^{zc/melt}D_{La}$ and $^{zc/melt}D_{Yb}$ on melt evolution, using values determined by the melt inclusion-mineral technique and from Fujimaki (1986). Also shown for comparison are model results without zircon in the residual assemblage for batch partial melting (a) and in the fractionation assemblage for fractional crystallization (b). The numbers next to the model values indicate the mass percent melt generated for partial melting and the mass percent crystallization for fractional crystallization. The La (16.1 ppm) and Yb (4.2 ppm) concentrations of the starting composition for the partial melting model are from a mafic (amphibolite) protolith (Thomas and Sinha 1999). The fractional crystallization model uses 96.6 ppm La and 4.38 ppm Yb (MI #4 from Thomas et al. 2002) as the starting concentrations. The partition coefficients for clinopyroxene and plagioclase are from Klein et al. (2000), Schnetzler and Philpotts (1970) and Fujimaki et al. (1984). [Used by permission of Elsevier Science, from Thomas et al. (2002) *Geochimica et Cosmochimica Acta*, Vol. 66, Fig. 9, p. 2898]

lected La and Yb for these calculations because published partition coefficients for these elements show the largest departure from results obtained using the MIM technique described above. Results using the MIM technique are compared to those of Fujimaki (1986) because those values are widely used in published petrogenetic models.

The La concentrations modeled by batch partial melting are not significantly different between the zircon-free and zircon-bearing models, or using the Fujimaki (1986) data or data obtained from the MIM technique. As shown on Figure 8a, Yb is most incompatible in the residue for the model with 0% zircon in the residual assemblage, as well as in the model including 0.5% zircon and using $^{zc/melt}D_{Yb}$ obtained from the MIM technique. However, using $^{zc/melt}D_{Yb}$ from Fujimaki (1986) results in Yb depletion in the melt for the zircon-bearing case. During fractional crystallization, Yb is conserved in the melt for the model with 0% zircon in the fractionated assemblage, as well as in the model including 0.5% zircon and using $^{zc/melt}D_{REE}$ obtained from the MIM technique (Fig. 8b). However, using $^{zc/melt}D_{REE}$ of Fujimaki (1986) results in strongly Yb-depleted melt for the zircon-bearing case. These calculations illustrate the significant differences that may result using different values for REE partition coefficients in petrogenetic models and highlight the need for accurate partitioning data for use in modeling.

Summary of trace element partitioning by the MIM technique

It is important to emphasize that partition coefficients in natural systems vary as a function of many parameters, including ionic potential, temperature, pressure, oxygen fugacity, crystal chemistry, and melt composition, including water content (Onuma et al. 1968, Drake and Weill 1975, Watson 1977, Matsui et al. 1977, Philpotts 1978, Hart and Davis 1978, Lindstrom and Weill 1978, Ryerson and Hess 1978, Green and Pearson 1983, 1986; Dunn 1987, Blundy and Wood 1991, Hill et al. 2000). For example, the volatile content of a melt may significantly affect partitioning behavior of trace elements between the melt and crystallizing phases. Wood and Blundy (2002) note that water has the effect of lowering $^{cpx/melt}D_{REE}$ but that water has no effect on $^{garnet/melt}D_{REE}$. Blundy (pers. comm. 2002) further notes that zircon may behave more like garnet. A great advantage of the MIM technique is that many of the parameters that may affect trace element partitioning can be measured directly by analysis of the MI. For instance, Thomas et al. (2002) estimated water contents as high as 8 to 9 wt % in zircon hosted MI, and some of the differences in partitioning behavior that they observed (compared to other published results) may be due to these high water contents.

Median zircon/melt D_{REE} determined from 11 zircon/MI pairs from the Toba rhyolite and from

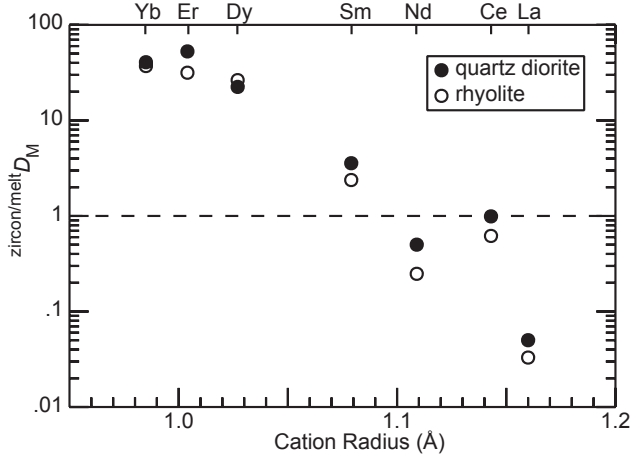

Figure 9. Comparison of $^{zc/melt}D_M$ determined from homogenized melt inclusions in zircons from the Quottoon quartz diorite and glass inclusions in zircons from the Toba rhyolite. Note that similar partition coefficients were obtained using both homogenized and glass melt inclusions in zircons. The dashed line is the same as in Figure 6a.

11 zircon/MI pairs from the Quottoon quartz diorite are shown on Figure 9. The median partition coefficients are remarkably similar even though the zircons were extracted from rocks with significantly different bulk rock compositions (62 wt % SiO_2 for the quartz diorite and 76 wt % SiO_2 for the rhyolite). Although the bulk rock compositions are very different, compositions of MI in zircon from these two rocks show much smaller differences. The similarity of the partition coefficients determined from zircon/MI pairs extracted from two different bulk rocks, from different types of MI (homogenized versus glass MI) provides strong evidence for the validity of the MIM technique for determining partition coefficients. The differences between the bulk rock composition and the melt inclusion compositions, perhaps, illustrate the dangers of using the bulk rock as a measure of the melt for determination of partitioning behavior. It is also important to note that the MI in zircons from the rhyolite were not heated, yet the partition coefficients determined using the MIM technique yielded essentially the same results as those obtained from the homogenized MI in zircons from the quartz diorite. The similarity of the partition coefficients from these two rocks indicates that the REE abundances of the homogenized MI were not changed during heating and homogenization experiments.

The MIM technique described above to determine trace element partition coefficients is valid for the mineral zircon. The validity of the technique is based on the fact that diffusion rates for REE in zircon are extremely slow (Cherniak et al. 1997, Cherniak and Watson, this volume). Thus, the REE concentrations of MI and host zircon are unlikely to change as a result of diffusion following trapping. However, similar behavior is not expected for all minerals from all environments. While Sobolev et al. (1996) were able to determine trace element partitioning behavior between basaltic melt and clinopyroxene based on MI in clinopyroxene from the Upper lavas of the Troodos Massif, Cyprus, it is not clear that the approach would have worked for clinopyroxene (or other minerals) that cooled more slowly in a deep-seated environment.

ARE MI COMPOSITIONS REPRESENTATIVE OF THE BULK MELT?

To use MI to better understand geologic processes, it must be assumed that the MI compositions are representative of the bulk melt. Below we consider several mechanisms that could produce MI with compositions different from that of the bulk melt at the time of trapping. First we address the possibility that MI compositions are not representative of the bulk melt due to boundary layer processes. Next, we consider if the MI remained a closed system since the time of formation and whether compositions of MI have changed by diffusive exchange with melt (or other fluids) outside the host crystal. Finally, we discuss potential analytical errors (homogenization of crystalline MI, and electron microprobe and SIMS analyses).

Boundary layer effects

A primary concern of MI studies is whether MI compositions are representative of the bulk melt (e.g., Watson et al. 1982, Bacon 1989). During crystal growth, compatible elements are depleted from the melt near the crystal-melt interface, and incompatible elements accumulate in the boundary layer because they are excluded from the growing crystal. The width of the boundary layer is governed by the crystal growth rate, the rate at which compatible elements diffuse towards a growing crystal and the rate at which incompatible elements diffuse away from the boundary layer. If a significant proportion of the MI is composed of melt from a chemically differentiated boundary layer, the MI composition may not be representative of the bulk melt. The scale of the boundary layer and its role in affecting MI trace element chemistry is poorly understood. If boundary layers have dimensions similar to melt inclusion sizes (i.e., tens of microns), then systematic variations between MI size and trace element concentration should be observed. Additionally, the extent of enrichment and depletion for different elements should vary from one host mineral to the next. Several studies addressed the significance of boundary layer development, and concluded that its effect on MI compositions is small for most inclusions greater than ~25 μm (Anderson 1974,

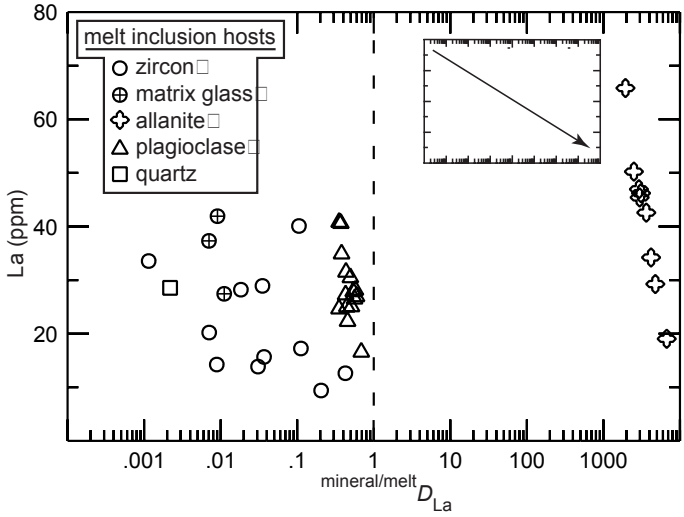

Figure 10. $^{Mineral/melt}D_{La}$ versus La contents of melt inclusions hosted by zircon, allanite, plagioclase and quartz from the Toba rhyolite. The arrow in the inset schematically shows the trend that would be expected if melt inclusion scale boundary layers had affected the trace element compositions of the inclusions. The mineral/melt partition coefficients were determined using the melt inclusion-mineral technique (see text). The dashed line is the same as in Figure 6a.

Lowenstern 1995) and can be ignored for inclusions >50 μm in diameter (Lu et al. 1995). Webster and Rebbert (2001) found no boundary layer effects in MI smaller than 70 μm in quartz from Ascension Island.

To better understand the role of boundary layers during MI formation, the trace element chemistry (La, Ce, Nd, Sm, Dy, Er, Yb and Sr) of MI in zircon, allanite, plagioclase and quartz from the Toba rhyolite was examined. Matrix glass adhering to zircon crystals was also analyzed. Based on petrographic evidence and major element chemistry, zircon, allanite, plagioclase and quartz co-crystallized from the same rhyolitic melt. Solid inclusions of each mineral occur in all the other minerals. For example, solid inclusions of zircon occur in allanite, plagioclase and quartz indicating that zircon was precipitating at the same time (and perhaps earlier) as the last mineral to crystallize from the melt. Major element concentrations of the MI in the different minerals overlap suggesting co-crystallization.

If boundary layers on the order of tens of microns developed adjacent to growing crystals, then MI in zircon should be enriched in the incompatible elements La, Nd and Sr compared to the bulk melt. Conversely, the heavy REE are compatible in zircon and should be depleted in the MI compared to the average melt. Melt inclusions in allanite crystals should be depleted in all REE (especially La), because the REE are highly compatible in the allanite crystal structure. REE^{3+} are incompatible in plagioclase, whereas, Sr is compatible in plagioclase. Therefore, all REE should be enriched in MI in plagioclase crystals compared to the bulk melt. REE and Sr are incompatible in quartz; thus, MI in quartz should contain higher concentrations of the trace elements than the bulk melt.

Results of SIMS analyses show that MI hosted by allanite are not depleted in La compared to MI hosted by zircon, plagioclase, or quartz (Fig. 10) as would be expected if a La-depleted boundary layer had affected MI compositions. Likewise, MI hosted by plagioclase are not depleted in Sr compared to MI in zircon, allanite or quartz as would be expected if a Sr-depleted boundary layer had affected MI compositions. The MI contained in quartz have lower concentrations of REE and Sr than MI hosted by zircon, allanite and plagioclase. Furthermore, there are no systematic variations in trace element concentrations as a function of MI size (Fig. 11) as would be expected if the compositions of MI were modified by boundary layer processes. Also, the La concentration of

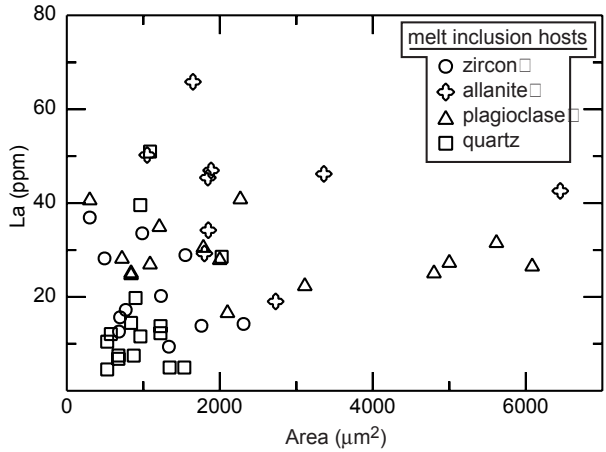

Figure 11. The La abundances of melt inclusions hosted in zircon, allanite, plagioclase and quartz crystals from the Toba rhyolite are not correlated with melt inclusion size, as would be expected if melt inclusion scale boundary layers had affected the trace element compositions of the inclusions. Melt inclusion cross-sectional area was calculated using the maximum dimensions of the melt inclusions.

matrix glass adhering to zircon is similar to MI hosted by zircons. We note that the inclusions described here range from 20 to 100 μm and do not preclude the possibility that boundary layer processes affect the compositions of smaller MI. Based on our studies of MI contained in minerals with significantly different partitioning behavior, we conclude that boundary layer processes did not affect the compositions of the MI contained in these crystals, and are probably insignificant in most MI studies.

Re-equilibration of melt inclusions

An additional assumption involved in the use of MI is that they remain closed systems after trapping. However, under some conditions and in some host minerals (e.g., olivine), melt trapped in an inclusion may continue to equilibrate with the bulk melt surrounding the host mineral as a result of diffusive exchange of components. For example, it is well known that water (Sobolev et al. 1990, Lowenstern and Mahood 1991, Lu 1991, Vityk et al. 2000) and some major elements (Gaetani and Watson 2000, Danyushevsky et al. 2000, 2002) in MI may continue to exchange with the host phase or surrounding melt, either during slow cooling in nature or during prolonged heating experiments in the laboratory. Qin et al. (1992) modeled the diffusive re-equilibration of chemical species in inclusions with the surrounding melt. For a host crystal 1 mm in diameter containing a 10 μm MI, it would take approximately 3×10^{14} years for Lu in a zircon hosted inclusion to reach 10% re-equilibration with the melt surrounding the crystal (based on the diffusion coefficient for Lu from Cherniak et al. 1997, Cherniak and Watson, this volume). The time required to reach a given degree of re-equilibration increases as the diffusion coefficient decreases. According to Cherniak et al. (1997), the diffusion coefficients for the REE in zircon decrease with decreasing atomic number; thus, the time required for all other REE will be longer than that calculated above for Lu. Thus, the theoretical model of Qin et al. (1992) indicates that the probability of changing the REE concentration of MI in zircon as a result of diffusion is essentially nil, even if the MI had been maintained at the formation temperature for hundreds of millions of years. Of course, rates of diffusion will be faster in most host phases other than zircon, and may significantly affect the MI composition. We also note that the diffusion coefficients for other trace elements (such as Ba, Rb, B, Sr, Ti Y and Nb described above) are not as well constrained as those for REE in zircon, and could have been modified by later processes.

The closure temperature for REE diffusion in zircon is higher than that for most other min-

erals, such as diopside, titanite, garnet and apatite (Dahl 1997, Cherniak et al. 1997), suggesting that inclusions in these minerals would continue to exchange REE with the melt surrounding the crystal to a lower temperature compared to zircon (Qin et al. 1992). Thus, the MIM technique should only be used to determine partition coefficients for trace elements in minerals with high closure temperatures for those elements, and/or from environments in which post-entrapment cooling was rapid.

Potential errors during homogenization and analysis

As discussed above, compositions of MI in zircons were unlikely to have been affected by boundary layer processes or diffusion-related re-equilibration following entrapment. This allows us to focus on errors resulting from homogenizing the inclusions, and analytical errors. During the course of heating inclusions to produce a homogeneous glass for microanalysis, it is assumed that any zircon that precipitated onto the MI walls following entrapment would have been incorporated back into the melt during the homogenization experiments. The amount of zircon precipitated during cooling (or dissolved during later reheating) is controlled by zircon solubility in the melt as a function of temperature (and melt composition). Good agreement between measured homogenization temperatures and temperatures predicted from the zircon saturation equation of Watson and Harrison (1983) (using the measured Zr concentrations in the MI), suggests that MI equilibrated with the zircon host during the homogenization process, i.e., all zircon precipitated during cooling was subsequently dissolved during heating to homogenize the MI.

To assess potential errors associated with dissolving too much or too little zircon host during homogenization, Thomas et al. (2002) compared MI homogenization temperatures to zircon saturation temperatures (Watson and Harrison 1983) calculated from compositions of inclusions. For example, one inclusion in zircon from the quartz diorite had 649 ppm Zr, an M-value of 1.26 (where M is the cation ratio [Na+K+2Ca]/Si·Al), and yielded a temperature (937°C) that is in excellent agreement with the measured homogenization temperature (950°C). If it is assumed that during cooling and crystallization all of the Zr in the original melt was incorporated into zircon crystallizing on the walls, and if only 10% (65 ppm) of the Zr that precipitated was re-incorporated into the melt during homogenization, then the calculated zircon saturation temperature would be 721°C. Similarly, overheating the inclusion and adding 1% excess zircon (containing ~500,000 ppm Zr) to the MI would change the Zr concentration in the melt from 649 to 5573 ppm. The zircon saturation temperature predicted from this Zr concentration is 1242°C. Note that dissolving excess zircon during homogenization is analogous to placing the ion beam partially on the MI and partially on the host zircon during SIMS analysis. Incorporation of excess zircon in the inclusion, either from overheating or incorrect beam placement, would result in a zircon saturation temperature significantly different from those calculated for the MI (and significantly different from the measured homogenization temperatures), and is not supported by the measured Zr concentrations of the MI.

FUTURE DIRECTIONS

Melt inclusions hold great promise as a tool to better understand geologic processes. As demonstrated by Chupin et al. (1998), MI hosted in detrital zircons may be a valuable tool (in addition to zircon ages and geochemical-isotopic data from the zircon crystal itself) to fingerprint sediment sources and help constrain tectonic reconstruction models. Melt inclusions should become a widely used tool in provenance studies to directly measure the compositions of zircon-precipitating melts. Wilde et al. (2001) used oxygen isotopic and trace element data from detrital zircons from western Australia to infer the existence of granitoid magmatism in Earth's early history at 4.404 Ga. As such, MI in old zircons may preserve compositions of ancient crust forming melts, providing direct measurement of melt chemistry and possibly revealing an unprecedented understanding of the Earth's early history.

In many cases it is difficult to infer the geologic environment in which a particular zircon

crystal grew, especially in rocks with polygenetic histories (e.g., growth from a melt versus hydrothermal growth; see Hoskin and Black (2000) for details regarding modes of zircon growth). It is important to note that inherited zircon cores are common in igneous zircons (but not in peralkaline rocks) (Vavra 1990) and have been identified through detailed microscopy (e.g., petrography, cathodoluminescence, back-scattered electron imaging) and/or differences in composition and age between core and overgrowth (Hanchar and Rudnick 1995). As discussed above, Chupin et al. (1998) documented that MI in 3.4 Ga zircons survived episodes of metamorphism that reached granulite facies in some rocks.

Assuming that a significant portion of all zircon that crystallized from a melt contain MI, the presence or absence of MI in zircon would not only verify (or refute) that the enclosing zircon precipitated from a melt, but would also yield the composition of the melt from which the zircon crystallized. Ideally, both an inherited zircon core and the overgrowth would contain MI if both crystallized from a melt. The MI in the core would yield the composition of the melt that crystallized to form the source region protolith that was later partially melted to form a new batch of magma. Melt inclusions in the zircon overgrowth would represent the zircon-precipitating melt that formed during (or after) partial melting of the source protolith. To date there have been no measurements of isotopic compositions of MI in zircon. An obvious application would be to use the isotopic compositions of MI in zircons to constrain melt source regions, models of magma mixing and assimilation/crystallization.

The position in the crystallization sequence represented by a particular MI is usually inferred by its SiO_2 content or some other fractionation index. To more accurately constrain the petrogenetic history of magmatic systems, it would be useful to combine geochemical/isotopic information from MI with the absolute ages of the host zircon using ^{238}U-^{230}Th disequilibrium ages. Such information would provide a method to assess melt compositional variations on an absolute time scale. Acquiring U-Th disequilibrium ages of MI host phases is most likely possible for U- and Th-rich accessory minerals like zircon (Reid et al. 1997, Lowenstern et al. 2000, Vasquez and Reid 2001) from rocks ranging in age from ~1 ka to ~1 Ma. As analytical techniques continue to become more miniaturized and as lower detection limits are achieved in mass spectrometry, zircon hosted MI investigations will allow us to answer many currently unresolved questions.

ACKNOWLEDGMENTS

The authors thank L. Fedele, J.J. Student, G. Benedix and R.J. Tracy for advice and assistance concerning electron microprobe analyses of glass inclusions. J.J. Student provided valuable advice on techniques for homogenizing crystalline melt inclusions. Constructive reviews by J.M. Hanchar and W. Van Westrenen greatly improved an earlier version of this manuscript. Funding was provided by grant EAR-0001168 from the National Science Foundation to R.J. Bodnar and A.K. Sinha.

REFERENCES

Anderson AT (1974) Evidence for a picritic, volatile-rich magma beneath Mt. Shasta, California. J Petrol 15:243-267

Anderson AT, Newman S, Williams SN, Druitt TH, Skirius C, Stolper E (1989) H_2O, CO_2, Cl and gas in Plinian and ash-flow Bishop rhyolitic tuff. Am Mineral 76:221-225

Bacon CR (1989) Crystallization of accessory phases in magmas by local saturation adjacent to phenocrysts. Geochim Cosmochim Acta 53:1055-1066

Barker F (1979) Trondhjemites: Definition, Environment and Hypothesis of Origin. *In* Barker F (ed) Trondhjemites, Dacites and Related Rocks. Elsevier, Amsterdam, p 1-12

Bea F (1996) Residence of REE, Y, Th and U in granites and crustal protoliths: implications for the chemistry of crustal melts. J Petrol 37:521-552

Bea F, Pereira MD, Stroh A (1994) Mineral/leucosome trace-element partitioning in a peraluminous migmatite (a laser ablation-ICP-MS study). Chem Geol 117:291-312

Beattie P (1994) Systematics and energetics of trace-element partitioning between olivine and silicate melts: Implications for the nature of mineral/melt partitioning. Chem Geol 117:57-71

Blundy JD, Wood BJ (1991) Crystal-chemical controls on the partitioning of Sr and Ba between plagioclase feldspars, silicate melts and hydrothermal solutions. Geochim Cosmochim Acta 55:193-209
Blundy JD, Wood BJ (1994) Prediction of crystal-melt partition coefficients from elastic moduli. Nature 372:452-454
Brice JC (1975) Some thermodynamic aspects of the growth of strained crystals. J Cryst Growth 28:249-253
Cherniak DJ, Hanchar JM, Watson EB (1997) Rare-earth diffusion in zircon. Chem Geol 134:289-301
Chesner CA (1998) Petrogenesis of the Toba Tuffs, Sumatra, Indonesia. J Petrol 39:397-438
Chupin SV, Chupin VP, Barton JM, Barton ES (1998) Archean melt inclusions in zircon from quartzite and granitic orthogneiss from South Africa: magma compositions and probable sources of protoliths. Eur J Mineral 10:1241-1251
Cox KG, Bell JD, Pankhurst RJ (1979) The Interpretation of Igneous Rocks. George, Allen and Unwin, London
Dahl PS (1997) A crystal-chemical basis for Pb retention and fission-track annealing systematics in U-bearing minerals, with implications for geochronology. Earth Planet Sci Lett 150:277-290
Danyushevsky LV, Della-Pasqua FN, Sokolov S (2000) Re-equilibration of melt inclusions trapped by magnesian olivine phenocrysts from subduction-related magmas: petrological implications. Contrib Mineral Petrol 138:68-83
Danyushevsky LV, McNeill AW, Sobolev AV (2002) Experimental and petrological studies of melt inclusions in phenocrysts from mantle-derived magmas: an overview of techniques, advantages and complications. Chem Geol 183:5-24
Drake MJ, Weill DF (1975) Partition of Sr, Ba, Ca, Y, Eu^{2+}, Eu^{3+}, and other REE between plagioclase feldspar and magmatic liquid: an experimental study. Geochim Cosmochim Acta 39:689-712
Dunn T (1987) Partitioning of Hf, Lu, Ti, and Mn between olivine, clinopyroxene and basaltic liquid. Contrib Mineral Petrol 96:476-484
Finch RJ, Hanchar JM, Hoskin PWO, Burns PC (2001) Rare earth elements in synthetic zircon: Part 2. A single-crystal X-ray study of xenotime substitution. Am Mineral 86:681-689
Frezzotti ML (2001) Silicate-melt inclusions in magmatic rocks: applications to petrology. Lithos 55:273-299
Fujimaki H (1986) Partition coefficients of Hf, Zr, and REE between zircon, apatite, and liquid. Contrib Mineral Petrol 94:42-45
Fujimaki H, Tatsumoto M, Aoki K (1984) Partition coefficients of Hf, Zr and REE between phenocrysts and groundmass. J Geophys Res 89:B662-B672.
Gaetani GA, Watson EB (2000) Open system behavior of olivine-hosted melt inclusions. Earth Planet Sci Lett 183:27-41
Green TH, Pearson NJ (1983) Effect of pressure on rare earth element partition coefficients in common magmas. Nature 305:414-416
Green TH, Pearson NJ (1986) Rare-earth element partitioning between sphene and coexisting silicate liquid at high pressure and temperature. Chem Geol 55:105-119
Greenland LP (1970) An equation for trace element distribution during magmatic crystallization. Am Mineral 55:455-465
Guo J, O'Reilly SY, Griffin WL (1996) Zircon inclusions in corundum megacrysts: I. Trace element geochemistry and clues to the origin of corundum megacrysts in alkali basalts. Geochim Cosmochim Acta 60:2347-2363
Halter WE, Pettke T, Heinrich CA, Rothen-Rutishauser B (2002) Major to trace element analysis of melt inclusions by laser-ablation ICP-MS: methods of quantification. Chem Geol 183:63-86
Hanchar JM, Rudnick RL (1995) Revealing hidden structures: the application of cathodoluminescence and back-scattered electron imaging to dating zircons from lower crustal xenoliths. Lithos 36:289-303
Hanchar JM, Finch RJ, Hoskin PWO, Watson EB, Cherniak DJ, Mariano AN (2001) Rare earth elements in synthetic zircon: Part 1. Synthesis, and rare earth element and phosphorous doping. Am Mineral 86:667-680
Hart SR, Davis KE (1978) Nickel partitioning between olivine and silicate melt. Earth Planet Sci Lett 40:203-219
Hazen RM, Finger LW (1979) Bulk modulus-volume relationship for cation-anion polyhedra. J Geophys Res 84:6723-6728
Hervig RL, Dunbar NW (1992) Causes of chemical zoning in the Bishop (California) and Bandelier (New Mexico) magma chambers. Earth Planet Sci Lett 111:97-108
Hervig RL, Dunbar NW, Westrich HR, Kyle P (1989) Pre-eruptive water content of rhyolitic magmas as determined by ion microprobe analyses of melt inclusions in phenocrysts. J Volc Geotherm Res 36:293-302
Hill E, Wood BJ, Blundy JD (2000) The effect of Ca-Tschermaks component on trace element partitioning between clinopyroxene and silicate melt. Lithos 53:203-215
Hinton RW, Myer C (1991) Ion probe analysis of zircon and yttrobetafite in a lunar granite. Lunar Planet Sci XXII:575-576
Hinton RW, Upton BGJ (1991) The chemistry of zircon: Variations within and between large crystals from syenite and alkali basalt xenoliths. Geochim Cosmochim Acta 55:3287-3302
Hoskin PWO, Black LP (2000) Metamorphic zircon formation by solid-state recrystallization of protolith igneous zircon. J Metamor Geol 18:423-439
Hoskin PWO, Kinny PD, Wyborn D, Chappell BW (2000) Identifying accessory mineral saturation during differen-

tiation in granitoid magmas: an integrated approach. J Petrol 41:1365-1396
Ihinger PD, Hervig RL, McMillan PF (1994) Analytical methods for volatiles in glasses. Rev Mineral 30:67-121
Ireland TR, Wlotzka F (1992) The oldest zircons in the solar system. Earth Planet Sci Lett 109:1-10
Kamenetsky VS, Crawford AJ, Eggins SM, Muehe R (1997) Phenocryst and melt inclusion chemistry of near-axis seamounts, Valu Fa Ridge, Lau Basin: insight into mantle wedge melting and the addition of subduction components. Earth Planet Sci Lett 151:205-223
Klein M, Stosch H-G, Seck HA, Shimizu N (2000) Experimental partitioning of high field strength and rare earth elements between clinopyroxene and garnet in andesitic andtonalitic systems. Geochim Cosmochim Acta 64:99-115.
Li Z (1994) The silicate melt inclusions in igneous rocks. *In* De Vivo B, Frezzotti ML (eds) Fluid Inclusions in Minerals: Methods and Applications. Virginia Tech, Blacksburg, Virginia, p 73-94
Lindstrom DJ, Weill DF (1978) Partitioning of transition metals between diopside and coexisting silicate liquids: I. Nickel, cobalt, and manganese. Geochim Cosmochim Acta 42:817-832
Lowenstern JB (1994) Dissolved volatile concentrations in an ore-forming magma. Geology 22:893-896
Lowenstern JB (1995) Applications of silicate-melt inclusions to the study of magmatic volatiles. *In* Thompson FH (ed) Magma, Fluids, and Ore Deposits. Mineral Assoc Canada, Short Course Ser 23:71-99
Lowenstern JB, Mahood G (1991) New data on magmatic H_2O contents of pantellerites, with implications for petrogenesis and eruptive dynamics at Pantelleria. Bull Volcanol 54:78-83
Lowenstern JB, Persing HM, Wooden JL, Lanphere M, Donnely-Nolan J, Grove TL (2000) U-Th dating of single zircons from young granitoid xenoliths: new tools for understanding volcanic processes. Earth Planet Sci Lett 183:291-302
Lu F (1991) The Bishop Tuff: Origin of the high-silica rhyolite and its thermal and compositional zonations. PhD dissertation, University of Chicago, Chicago, Illinois
Lu F, Anderson AT, Davis AM (1992) New and larger sanidine/melt partition coefficients for Ba and Sr as determined by ion microprobe analyses of melt inclusions and their sanidine host crystals. Geol Soc Am Abstr Progr 24:A44
Lu F, Anderson AT, Davis AM (1995) Diffusional gradients at the crystal/melt interface and their effect on the compositions of melt inclusions. J Geol 103:591-597
Maas R, Kinny PD, Williams IS, Froude DO, Compston W (1992) The Earth's oldest known crust: A geochronological and geochemical study of 3900 Ma detrital zircons from Mt. Narryer and Jack Hills, western Australia. Geochim Cosmochim Acta 56:1281-1300
Mahood G, Hildreth W (1983) Large partition coefficients for trace elements in high-silica rhyolites. Geochim Cosmochim Acta 47:11-30
Matsui Y, Onuma N, Nagasawa H, Higuchi H, Banno S (1977) Crystal structure control in trace element partition between crystal and magma. Bull Soc Fr Minéral Cristallogr 100:315-324
Michael PJ (1988) Partition coefficients for rare earth elements in mafic minerals of high silica rhyolites: The importance of accessory mineral inclusions. Geochim Cosmochim Acta 52:275-282
Morgan GB, London D (1996) Optimizing the electron microprobe analysis of hydrous alkali aluminosilicate glasses. Am Mineral 81:1176-1185
Murali AV, Parthasarathy R, Mahadevan TM, Sankar D (1983) Trace element characteristics, REE patterns and partition coefficients of zircons from different geological environments-A case study on Indian zircons. Geochim Cosmochim Acta 47: 2047-2052
Nagasawa, H (1970) Rare earth concentrations in zircon and their host dacites and granites. Earth Planet Sci Lett 9:359-364
Nakamura N (1974) Determination of REE, Ba, Fe, Mg, Na, and K in carbonaceous and ordinary chondrites. Geochim Cosmochim Acta 38:757-775
Nielsen TFD, Solovova IP, Veksler IV (1997) Parental melts of melilitolite and origin of alkaline carbonatite: evidence from crystallized melt inclusions, Gardiner Complex. Contrib Mineral Petrol 126:331-344
O'Hara MJ, Fry N, Prichard HM (2001) Minor phases as carriers of trace elements in non-modal crystal-liquid separation processes II: illustrations and bearing on behaviour of REE, U, Th and the PGE in igneous processes. J Petrol 42:1887-1910
Onuma N, Higuchi H, Wakita H, Nagasawa H (1968) Trace element partitioning between two pyroxenes and the host lava. Earth Planet Sci Lett 5:47-51
Philpotts JA (1978) The law of constant rejection. Geochim Cosmochim Acta 42:909-920
Poldervaart A (1955) Zircon in rocks: 1, sedimentary rocks. Am J Sci 253:433-461
Poldervaart A (1956) Zircon in rocks: 2, igneous rocks. Am J Sci 254:521-554
Pupin JP, Turco G (1972) Une typologie originale du zircon accessoire. Bull Soc Fr Minéral Cristallogr 95:348-359
Qin Z, Fangqiong F, Anderson AT (1992) Diffusive reequilibration of melt and fluid inclusions. Am Mineral 77:565-576
Reid MR, Coath CD, Harrison TM, McKeegan KD (1997) Prolonged residence times for the youngest rhyolites associated with Long Valley Caldera: ^{230}Th-^{238}U ion microprobe dating of young zircons. Earth Planet Sci Lett 150:27-39

Roedder E (1979) Origin and significance of magmatic inclusions. Bull Minéral 102:487-510
Roedder E (1984) Fluid Inclusions. Rev Mineral, Vol 12, 644 p
Ryerson FJ, Hess PC (1978) Implications of liquid-liquid distribution coefficients to mineral-liquid partitioning. Geochim Cosmochim Acta 42:921-932
Schmidt C, Chou I-M, Bodnar RJ, Basset WA (1998) Microthermal analysis of synthetic fluid inclusions in the hydrothermal diamond anvil cell. Am Mineral 83:995-1007
Schnetzler CC, Philpotts JA (1970) Partition coefficients of rare earth elements between igneous matrix material and rock-forming mineral phenocrysts-II. Geochim Cosmochim Acta 34:331-340.
Schreibber HD, Lauer HV, Thanyasir T (1980) The redox state of cerium in basaltic magmas: An experimental study of iron-cerium interactions in melts. Geochim Cosmochim Acta 44:1599-1612
Shannon RD (1976) Revised effective ionic radii and systematic studies of interatomic distances in halides and chalcogenides. Acta Crystallogr A32:751-767
Shaw DM (1970) Trace element fractionation during anatexis. Geochim Cosmochim Acta 34:237-243
Shimizu N (1998) The geochemistry of olivine-hosted melt inclusions in a FAMOUS basalt ALV519-4-1. Phys Earth Planet Inter 107:183-201
Shimizu N, Hart S (1982) Applications of the ion microprobe to geochemistry and cosmochemistry. Ann Rev Earth Planet Sci 10:483-526
Shimizu N, Sobolev NV, Yefimova ES (1997) Chemical heterogeneities of inclusions in garnet and juvenile character of peridotitic diamonds from Siberia. Russ Geol Geophys 38:356-372
Sisson TW, Layne GD (1993) H_2O in basalt and basaltic andesite glass inclusions from four subduction-related volcanoes. Earth Planet Sci Lett 117:619-635
Sobolev AV (1996) Melt inclusions in minerals as a source of principle petrologic information. Petrology 4:209-220
Sobolev AV, Danyushevsky LV (1994) Petrology and geochemistry of boninites from the north termination of the Tonga Trench: constraints on the generation conditions of high-Ca boninite magmas. J Petrol 35:1183-1211
Sobolev AV, Shimizu N (1993) Ultra-depleted primary melt included in an olivine from the Mid-Atlantic Ridge. Nature 363:151-154
Sobolev AV, Kamenetsky VS, Metrich N, Clochiatti R, Konokova NN, Devirts AL, Ustinov VI (1990) Volatile regime and crystallization conditions in Etna Hawaiite lavas. Geochem Intl 990:53-65
Sobolev AV, Migdisov AA, Portnyagin MV (1996) Incompatible element partitioning between clinopyroxene and basaltic liquid revealed by study of melt inclusions in minerals from Troodos Lavas, Cyprus. Petrology 4:307-317
Sobolev VS, Kostyuk VP (1975) Magmatic crystallization based on a study of melt inclusions. Fluid Inclusion Res 9:182-253 (translated from original publication in Russian)
Sokolov S (2002) Melt inclusions as indicators of the magmatic origin of carbonatite rare metal and rare earth minerals. Chem Geol 183:373-378
Spandler CJ, Eggins SM, Arculus RJ, Mavrogenes JA (2000) Using melt inclusions to determine parent-magma compositions of layered intrusions: application to the Greenhills Complex (New Zealand), a platinum group minerals-bearing, island-arc intrusion. Geology 28:991-994
Speer JA (1982) Zircon. *In* Ribbe PH (ed) Orthosilicates. Rev Mineral 5:67-112
Student JJ, Bodnar RJ (1996) Melt inclusion microthermometry: petrologic constraints from the H_2O-saturated haplogranite system. Petrology 4:310-325
Taylor SR, McLennan SM (1981) The composition and evolution of the continental crust: rare earth element evidence from sedimentary rocks. Phil Tran R Soc A301:381-399
Thomas JB, Bodnar RJ (2002) A technique for mounting and polishing melt inclusions in small (<1 mm) crystals. Am Mineral 87:1505-1508
Thomas JB, Sinha AK (1999) Field, geochemical, and isotopic evidence for magma mixing and AFC processes in the Quottoon Igneous Complex, northwestern British Columbia and southeastern Alaska. Can J Earth Sci 36:819-831
Thomas JB, Bodnar RJ, Shimizu N, Sinha AK (2002) Determination of zircon/melt trace element partition coefficients from SIMS analysis of melt inclusions in zircon. Geochim Cosmochim Acta 66:2887-2901
Thomas R (1994) Estimation of viscosity and water content of silicate melts from melt inclusion data. Eur J Mineral 6:511-535
Thomas R (2000) Determination of water contents of granite melt inclusions by confocal laser Raman microprobe spectroscopy. Am Mineral 85:868-872
Van Westrenen W, Allan NL, Blundy JD, Purton JA, Wood BJ (2000) Atomistic simulation of trace element incorporation into garnets: comparison with experimental garnet-melt partitioning data Geochim Cosmochim Acta 64:1629-1639
Vasquez JA, Reid MR (2001) Timescales of magmatic evolution by coupling core-to-rim ^{238}U-^{230}Th ages and chemical compositions of mineral zoning in allanite from the Youngest Toba Tuff. EOS Trans, Am Geophys Union 82:F1019
Vavra G (1990) On the kinematics of zircon growth and its petrogenetic significance: a cathodoluminescence study.

Contrib Mineral Petrol 106:90-99
Vityk MO, Bodnar RJ, Doukhan JC (2000) Synthetic fluid inclusions XV. TEM investigation of plastic flow associated with reequilibration of fluid inclusions in natural quartz. Contrib Mineral Petrol 56:119-134
Watson EB (1977) Partitioning of Mn between forsterite and silicate liquid. Geochim Cosmochim Acta 41:1363-1374
Watson EB (1980) Some experimentally determined zircon/liquid partition coefficients for the rare earth elements. Geochim Cosmochim Acta 44:895-897
Watson EB (1996) Dissolution, growth and survival of zircons during crustal fusion: Kinetic principles, geologic models and implications for isotopic inheritance. Proc Roy Soc Edinburgh 8:43-56
Watson EB, Harrison TM (1983) Zircon saturation revisited: temperature and composition effects in a variety of crustal magma types. Earth Planet Sci Lett 64:295-304
Watson EB, Sneeringer MA, Ross A (1982) Diffusion of dissolved carbonate in magmas: experimental results and applications. Earth Planet Sci Lett 61:346-358
Webster JD, Duffield WA (1991) Volatiles and lithophile elements in Taylor Creek Rhyolite: Constraints from glass inclusion analysis. Am Mineral 76:1628-1645
Webster JD, Rebbert CR (2001) The geochemical signature of fluid-saturated magma determined from silicate melt inclusions in Ascension Island granite xenoliths. Geochim Cosmochim Acta 65:123-136
Wilde SA, Valley JW, Peck WH, Graham CM (2001) Evidence from detrital zircons for the existence of continental crust and oceans on the Earth 4.4 Gyr ago. Nature 409:175-178
Wood BJ, Blundy JD (1997) A predictive model for rare earth element partitioning between clinopyroxene and anhydrous silicate melt. Contrib Mineral Petrol 129:166-181
Wood BJ, Blundy JD (2002) The effect of H_2O on crystal-melt partitioning of trace elements. Geochim Cosmochim Acta 66:3647-3656
Wopenka B, Jolliff BL, Zinner E, Kremser D (1996) Trace element zoning and incipient metamictization in a lunar zircon: application of three microprobe techniques. Am Mineral 81:902-912